Inorganic Chemistry

Article

pubs.acs.org/IC

Sulfonyl-Substituted Heteroleptic Cyclometalated Iridium(III) Complexes as Blue Emitters for Solution-Processable Phosphorescent Organic Light-Emitting Diodes

Helen Benjamin,[†] Yonghao Zheng,[†] Andrei S. Batsanov,[†] Mark A. Fox,[†] Hameed A. Al-Attar,[‡] Andrew P. Monkman,[‡] and Martin R. Bryce*[,†]

[†]Department of Chemistry and [‡]Department of Physics, Durham University, Durham DH1 3LE, U.K.

Supporting Information

ABSTRACT: The synthesis is reported of a series of blue-emitting heteroleptic iridium complexes with phenylpyridine (ppy) ligands substituted with sulfonyl, fluorine, and/or methoxy substituents on the phenyl ring and a picolinate (pic) ancillary ligand. Some derivatives are additionally substituted with a mesityl substituent on the pyridyl ring of ppy to increase solubility. Analogues with two ppy and one 2-(2′-oxyphenyl)pyridyl (oppy) ancillary ligand were obtained by an unusual in situ nucleophilic displacement of a fluorine substituent on one of the ppy ligands by water followed by N^O chelation to iridium. The X-ray crystal structures of seven of the complexes are reported. The photophysical and electrochemical properties of the complexes are supported by density functional theory (DFT) and time-dependent DFT calculations. Efficient blue phosphorescent organic light-emitting devices (PhOLEDs) were fabricated using a selection of the complexes in a simple device architecture using a solution-processed single-emitting layer in the configuration ITO/PEDOT:PSS/PVK:OXD-7(35%):Ir complex(15%)/TPBi/LiF/Al. The addition of a sulfonyl substituent blue-shifts the electroluminescence by ca. 12 nm to λ_{max}^{EL} 463 nm with CIE$_{x,y}$ coordinates (0.19, 0.29), compared to the benchmark complex FIrpic (λ_{max}^{EL} 475 nm, 0.19, 0.38) in directly comparable devices, confirming the potential of the new complexes to serve as effective blue dopants in PhOLEDs. Replacing a fluorine by a methoxy group in these complexes red shifts the PL and EL λ_{max} by ca. 4−6 nm. The efficiency of the blue PhOLEDs of the sulfonyl-substituted complexes is, in most cases, significantly enhanced by the presence of a mesityl substituent on the pyridyl ring of the ppy ligands.

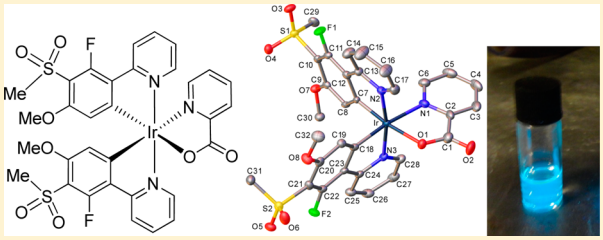

INTRODUCTION

Luminescent transition metal complexes are widely exploited in many areas,[1] such as biological labeling probes, ion sensors, water splitting, solar cells, and phosphorescent emitters for organic light-emitting diodes (OLEDs)[2−8] and for solid-state lighting.[9,10] In the OLED and lighting field cyclometalated iridium(III) complexes have received special attention because they can harvest both singlet and triplet excitons, leading to internal quantum efficiencies approaching 100%.[11−13] Key features of the complexes include their synthetic versatility, good color tuneability, generally good chemical and photochemical stability, relatively short excited-state lifetimes on the microsecond time scale, and highly efficient emission from a mixture of triplet metal-to-ligand charge-transfer (MLCT) states and $\pi-\pi^*$ transitions of the ligands.[14] Tris-homoleptic complexes [Ir(C^N)$_3$], where C^N is a monoanionic bidentate ligand, have been extensively studied, for example, the prototype green emitter *fac*-Ir(ppy)$_3$ (ppy = 2-phenylpyridine).[2] The highest occupied molecular orbital (HOMO) is primarily localized on the phenyl π and iridium d orbitals, while the lowest unoccupied molecular orbital (LUMO) resides mainly on the pyridine ring. Electron-withdrawing substituents, typically fluorine, are attached to the phenyl ring of the ppy ligands to blue-shift the emission by lowering the HOMO energy without significantly changing the LUMO energy.[15,16] For heteroleptic complexes [Ir(C^N)$_2$L] the ancillary ligand L can also be used to tune the emission color. The complex iridium(III) bis[4,6-(difluorophenyl)pyridinato-*N*,*C*-2′]-picolinate (FIrpic **1**; Figure 1) is the benchmark sky-blue emitter for phosphorescent OLEDs (PhOLEDs).[17−22] Other structural modifications that give blue emission involve different ancillary ligands such as N-heterocyclic carbenes,[23]

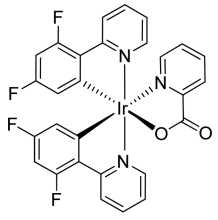

FIrpic **1**

Figure 1. Structure of FIrpic **1**.

Received: May 16, 2016
Published: August 11, 2016

DOI: 10.1021/acs.inorgchem.6b01179
Inorg. Chem. 2016, 55, 8612−8627

Scheme 1. Synthesis of Complexes 10−15[a]

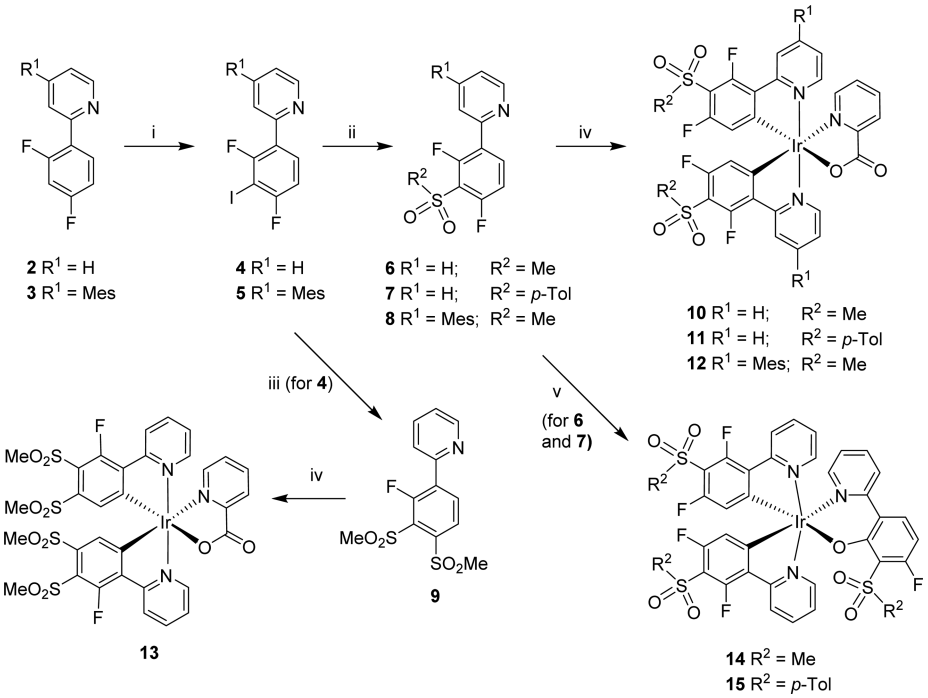

[a]Reagents and conditions: (i) LDA, THF, −78 °C, I_2, THF, 20 °C; (ii) $NaMeSO_2$ or Na*p*-$TolSO_2$, CuI, DMF, 110 °C; (iii) $NaMeSO_2$, CuI, I_2, DMF, 110 °C; (iv) $IrCl_3{\cdot}3H_2O$, 2-ethoxyethanol, 130 °C, followed by picolinic acid, 130 °C; (v) $IrCl_3{\cdot}3H_2O$, 2-ethoxyethanol, 130 °C, followed by ligand **6** or **7**, NEt_3, acetylacetone, ethylene glycol, 190 °C.

pyridylazolate derivatives,[24] fluorine-substituted bipyridine chelates,[25] and dicyclometalated phosphate tripod ligands.[26] The motivation for the present work was provided by the high level of ongoing research to develop new blue-emitting phosphors.[27,28]

This article describes the synthesis and X-ray structural and optoelectronic characterization of a systematic series of analogues of FIrpic **1** in which the phenyl ring bears a sulfonyl substituent at the C3 position to further lower the HOMO energy and blue-shift the emission. Additionally, we report derivatives with one or both of the fluorine atoms at C2 and C4 replaced by a methoxy group. The rationale here is that substituting one fluorine with an alkoxy group is known to have a minimal effect on the emission color while increasing the chemical stability of the complex to unwanted nucleophilic substitution reactions[29,30] during, or after, complex formation.[31] It is also known that di/multifluorinated ligands can degrade during OLED operation.[32] In some of the complexes a mesityl substituent is attached to C4 of the pyridyl ring, as it has been reported that this functionalization leads to enhanced PhOLED efficiency,[33] which is also the case for several complexes in the present work. The experimental photophysical and electrochemical data are supported by time-dependent density functional theory (TD-DFT) calculations. Blue PhOLEDs were fabricated with selected complexes as the emitter.

RESULTS AND DISCUSSION

It has been established previously that functionalizing the phenyl ring of FIrpic **1** with an electron-withdrawing group at C3 (i.e., between the two F atoms) induces a blue shift in emission: examples are cyano,[34] sulfonyl,[35e] phosphoryl,[35e] and perfluoroalkyl carbonyl substituents.[24b] The present work focuses on sulfonyl groups, which have only rarely been incorporated as substituents on C^N cyclometallating ligands in either neutral[35] or ionic[36] complexes. With the exception of complex **11**, which has been reported previously by Fan et al. using a different method to introduce the *p*-toluenesulfonyl substituent,[35e] to our knowledge the sulfone-containing complexes studied in this work have not been synthesized previously. The synthetic routes to complexes **10**−**15**, **23**−**25**, and **31** are shown in Schemes 1−3. All the complexes are characterized by NMR spectroscopy, mass spectrometry, and elemental analysis, with additional single-crystal X-ray crystallographic data for seven of the complexes.

The key step to introduce the sulfone substituent involves lithiation of 2-(2,4-difluorophenyl)pyridine **2**[37] or the mesityl analogue **3** with lithium diisopropylamide (LDA), followed by iodination to yield **4** and **5** and then reaction with either sodium *p*-toluenesulfinate or sodium methylsulfinate in the presence of stoichiometric copper(I) iodide, to afford ligands **6**−**8** in 15−26% yields (Scheme 1). These yields were highly reproducible in several reactions and could not be improved by ultilising a copper(II) bis(arylsulfinate) reagent,[38] a CuI/L-proline system,[39] or ionic liquid additives.[40] On one occasion, when using a batch of **4** that had not been rigorously purified (and was probably contaminated with iodine from the previous reaction) the di(methanesulfonyl) derivative **9** was also isolated in 11% yield alongside product **6**. When the reaction was repeated with rigorously purified **4** and the addition of a trace of iodine, compound **9** was again obtained in very low yield. Exploring the mechanism of this reaction is outside the scope of this work. However, it can be postulated: (i) that iodine coordinates to the pyridyl N atom of ligand **4** or **6** to form a more electron-withdrawing pyridinium unit, thereby further increasing the reactivity (by increased electron deficiency) of the phenyl ring, or (ii) that a fluorine in ligand **4** or **6** is

DOI: 10.1021/acs.inorgchem.6b01179
Inorg. Chem. 2016, 55, 8612−8627

Scheme 2. Synthesis of Complexes 23−25[a]

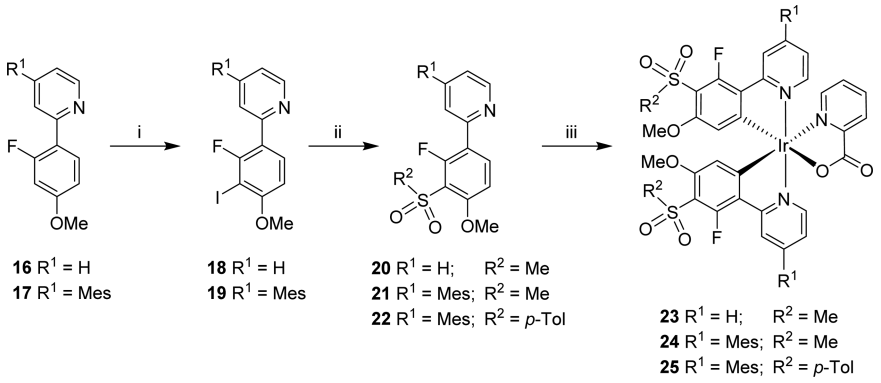

[a]Reagents and conditions: (i) LDA, THF, −78 °C, I_2, THF, 20 °C; (ii) $NaMeSO_2$ or Na*p*-$TolSO_2$, CuI, DMF, 110 °C; (iii) $IrCl_3{\cdot}3H_2O$, 2-ethoxyethanol, 130 °C, followed by picolinic acid, 130 °C.

Scheme 3. Synthesis of Complex 31[a]

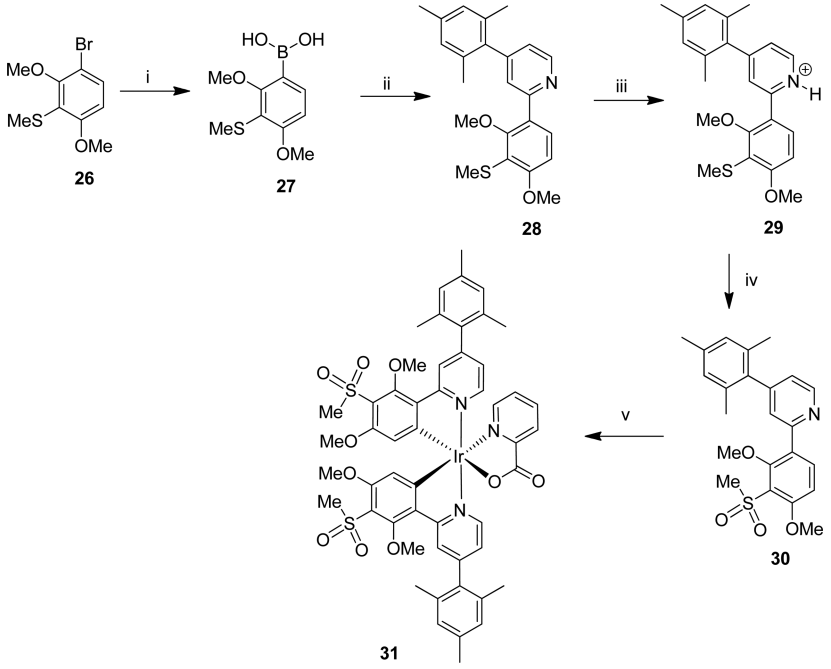

[a]Reagents and conditions: (i) *n*-BuLi, hexane, THF, −78 °C, triisopropyl borate, −78 to 20 °C, dilute HCl; (ii) 2-chloro-4-mesitylpyridine, PPh_3, DME, Na_2CO_3, $Pd(OAc)_2$, reflux; (iii) HCl, DCM/MeOH, RT; (iv) mcpba, DCM, 20 °C, $NaHSO_3$; (v) $[Ir(cod)Cl]_2$, 2-ethoxyethanol, 130 °C, followed by picolinic acid, 130 °C.

replaced by iodine prior to the reaction with the methylsulfinate anion. There is precedent for a combination of fluoro and iodo substituents on a phenyl ring facilitating S_NAr reactions at a C−F bond.[41]

The synthesis of methoxy analogues **23−25** followed a similar protocol starting from phenylpyridine derivatives **16** and **17**, which were readily obtained by standard Suzuki reactions of the commercially available 2-fluoro-4-methoxyphenylboronic acid (Scheme 2). Notably, the conversions of **18** and **19** to yield methanesulfonyl derivatives **20** and **21** proceeded in significantly higher yields (45 and 53%, respectively) than the comparable reactions of the difluoro analogues **4** and **5** in Scheme 1. However, the yield of *p*-tolyl derivative **22** is still low (21%).

To explore the effect of replacing both fluorine atoms with methoxy substituents, complex **31** was synthesized. To obtain the dimethoxy ligand **30**, a different synthetic approach was used starting from the known compound **26**[42] (Scheme 3). In this case, the sulfone functionality was obtained by oxidation of the methylthio group of **29** with *meta*-chloroperbenzoic acid in 83% yield.

To obtain the picolinate complexes **10−13**, **23−25**, and **31** standard conditions were employed,[43] namely, reaction of the ligand with $IrCl_3{\cdot}3H_2O$ (or $[Ir(cod)Cl]_2$ for **31**) in 2-ethoxyethanol to give a presumed bridged μ-dichloro diiridium species $[Ir(L)_2Cl]_2$, which was reacted in situ with picolinic acid. Attempts to isolate the intermediate dimer species were unsuccessful in most cases and usually led only to unidentified decomposed products. The attempted synthesis of **31** using $IrCl_3{\cdot}3H_2O$ failed to yield any product, and the ligand **30** could not be recovered. Difficulties in the cyclometalation of ligands

DOI: 10.1021/acs.inorgchem.6b01179
Inorg. Chem. 2016, 55, 8612−8627

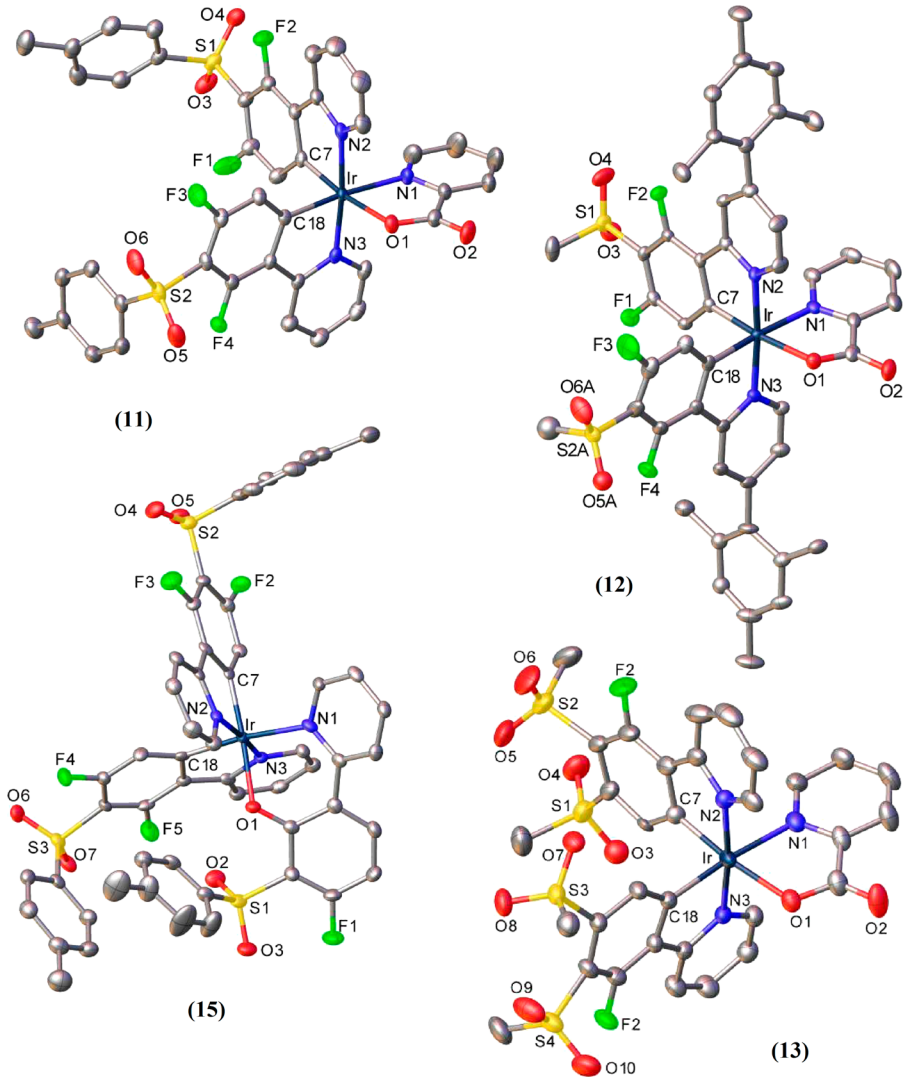

Figure 2. (a). X-ray molecular structures of **11**−**13** and **15**. Minor disorder components, solvent of crystallization, and all H atoms are omitted; thermal ellipsoids are drawn at the 50% probability level.

Table 1. Selected Bond Distances (Å)

	10	11	12	13	15	23	31
Ir−N(1)	2.137(3)	2.134(3)	2.140(5)	2.128(3)	2.161(4)	2.129(4)	2.120(4)
Ir−N(2)	2.027(3)	2.048(3)	2.033(5)	2.048(4)[a]	2.032(4)	2.035(4)	2.031(4)
Ir−N(3)	2.046(3)	2.029(3)	2.033(5)	2.040(4)	2.037(4)	2.041(4)	2.037(4)
Ir−O(1)	2.146(2)	2.158(2)	2.133(4)	2.148(3)	2.151(3)	2.142(3)	2.145(4)
Ir−C(7)	1.974(3)	1.985(3)	1.986(6)	1.994(4)	1.982(5)	1.987(4)	1.993(5)
Ir−C(18)	1.991(4)	1.989(3)	2.000(6)	1.979(5)[a]	1.989(5)	1.990(4)	1.998(4)

[a]Weighted average for the disordered ligands.

containing methoxy substituents using $IrCl_3 \cdot 3H_2O$ have been reported previously.[30b]

Attempts to form the corresponding tris-cyclometalated homoleptic $[Ir(C^N)_3]$ complexes from **6** and **7** using established conditions,[31d] by adding more C^N chelate to the $[Ir(L)_2Cl]_2$ species, gave the unexpected and unusual $[Ir(C^N)_2(N^O)]$ complexes **14** and **15** in 29% and 23% yields, respectively. There was no sign of the homoleptic complexes after purification of the product mixture. The structures of **14** and **15** were tentatively assigned based on mass spectra combined with ^{19}F NMR spectra, which showed the presence of only five fluorine atoms, together with ^1H NMR and COSY spectra that established that a fluorine ortho to a pyridyl group had been replaced on one of the ligands. The structures were subsequently unambiguously confirmed by X-ray crystallography of **15** (see below). The phenyl ring of ligands **6** and **7** is highly electron-deficient due to the presence of pyridyl, fluorine, and sulfone substituents; therefore, an S_NAr reaction at a C−F bond is entirely reasonable, for example, reaction with residual water in the ethylene glycol sovent, with subsequent N^O chelation as a 2-(2′-oxyphenyl)pyridyl (oppy) ancillary ligand. We are not aware of a previous example of an Ir complex of an oxyphenylpyridyl ligand. Indeed, six-membered ring chelation to Ir with a bidentate N^O ancillary ring appears

DOI: 10.1021/acs.inorgchem.6b01179
Inorg. Chem. 2016, 55, 8612−8627

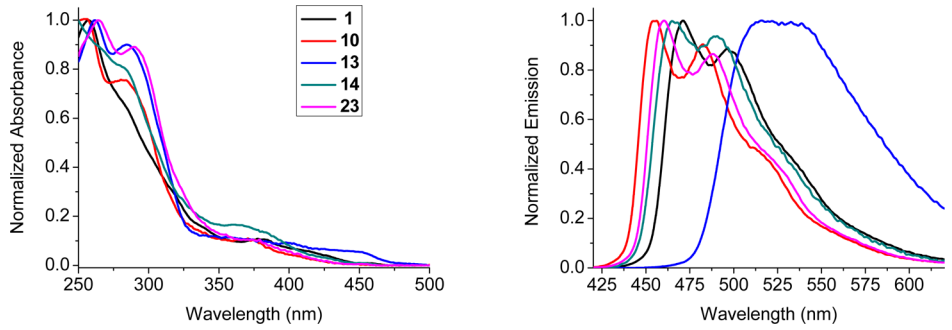

Figure 3. Normalized absorption (in dichloromethane, left) and emission (in degassed dichloromethane, right) solution-state spectra of complexes **1**, **10**, **13**, **14**, and **23**.

Table 2. Photophysical Data of the Iridium Complexes

complex	λ_{max}^{abs} (ε),[a] nm (1×10^3 $M^{-1}cm^{-1}$)	λ_{max}^{em},[b] nm	Stokes shift,[c] cm^{-1}	PLQY, Φ_{PL}[b,d]	τ_P,[b,e] μs
1 FIrpic	277 (50.1), 301 (34.2), 304 (32.6), 337 (13.8, sh), 357 (8.9, sh), 400 (6.2), 454 (0.8)	468, 496, 531 (sh)	800	0.67	1.72
10	255 (88.6), 282 (67.2), 292 (61.7), 371 (9.4), 401 (sh, 3.8), 443 (0.6)	455, 482, 511 (sh)	660	0.64	2.19
11	252 (123.7), 286 (90.4), 300 (83.0), 331 (sh, 23.4), 373 (11.3), 407 (sh, 4.7), 444 (0.8)	457, 483, 515 (sh)	700	0.68	2.09
12	260 (100.4), 283 (76.4), 321 (sh, 30.9), 374 (13.1), 401 (sh, 5.0), 444 (0.9)	457, 485, 517 (sh)	700	0.68	1.49
13	261 (89.1), 284 (80.2), 306 (b, 52.8), 399 (8.2), 452 (4.9), 490 (0.6)	516, 536	1450	0.48	3.53
14	264 (95.5), 278 (85.1), 302 (sh, 58.1), 364 (19.4), 382 (sh, 15.9), 421 (sh, 4.3), 447 (1.3)	466, 491, 530 (sh)	870	0.44	2.90
15	250 (sh, 143.2), 266 (sh, 98.7), 290 (83.4), 312 (56.5), 368 (19.6), 414 (sh, 6.7), 449 (1.4)	469, 494, 534 (sh)	910	0.38	2.85
23	253 (89.0), 264 (97.7), 290 (87.0), 319 (sh, 35.6), 372 (10.2), 406 (sh, 4.5), 449 (0.6)	460, 489, 522 (sh)	530	0.55	2.67
24	255 (99.0), 269 (118.1), 291 (110.6), 336 (sh, 27.6), 376 (15.9), 402 (sh, 6.8), 450 (0.9)	461, 489, 523 (sh)	530	0.58	1.79
25	258 (sh, 108.5), 271 (128.6), 297 (123.4), 307 (sh, 112.5), 339 (sh, 29.2), 379 (15.7), 450 (1.0)	464, 490, 524 (sh)	670	0.58	1.78
31	275 (104.4), 291 (101.9), 324 (sh, 47.8), 381 (14.5), 405 (sh, 7.9), 456 (0.9)	474, 500, 536 (sh)	830	0.50	2.13

[a]Data obtained in less than 10 μM dichloromethane solutions at 20 °C. [b]Data obtained in degassed dichloromethane solution with excitation wavelength at 380 nm. [c]Energy difference between lowest energy excitation maxima and highest energy excitation maxima. [d]Measured relative to $Ir(ppy)_3$ Φ_{PL} = 0.46 in degassed dichloromethane at 20 °C; estimated error ±5%. [e]Estimated error ±5%.

to be very rare:[14b] related examples include $[Ir(C^N)_2(N^O)]$ structures with two ppy ligands and 2-(2′-oxyphenyl)oxazole[44] or 2-(2′-oxyphenyl)oxazoline[45] as the ancillary N^O ligand.

X-ray Crystal Structures. Single-crystal X-ray structures were obtained for **10**, **11**·$3CH_2Cl_2$, **12**·$2.75CH_2Cl_2$, **13**·MeCN, **15**·$2CH_2Cl_2$·0.85MeOH, **23**·CH_2Cl_2, and **31**·$4CH_2Cl_2$ (Figures 2 and S1–S6 and Table S1). A different polymorph of **11**·$3CH_2Cl_2$ with essentially the same molecular geometry has been reported previously by Fan et al.[35e] In all the complexes, the Ir atom has a slightly distorted octahedral coordination. Table 1 lists bond lengths of all the structures with two C^N ligands and one N^O picolinate ligand.

The N atoms of the two C^N ligands are coordinated *trans* to each other. The picolinate ligand, as well as oppy ligand in **15**, forms a longer Ir–N bond, due to *trans*-effect of the σ-bonded C atom. In molecule **12**, the methylsulfonyl and mesityl groups of one C^N ligand are both disordered between two orientations in a 0.55:0.45 ratio (the Mes by a flipping motion). The Mes groups are nearly perpendicular to the adjacent Py rings, the dihedral angles being 86° for the ordered Mes group, 82° and 73° for the disordered Mes groups. In structure **13**, one whole C^N ligand is disordered between two orientations differing by a ca. 10° libration around the Ir atom, with occupancies refined to 0.684(5) and 0.316(5), respectively. All the chelating ligands show small but significant nonplanarity. In the picolinato ligand, the dihedral angle between the Py and carboxylate planes varies from 0.9° in **13** to 10.6° in **12**. In the C^N ligands, the twists between the phenyl and pyridine rings are the highest in complex **23** (12.7° and 14.7°), in other complexes they vary from 2° to 11°. The oxyphenyl-pyridine moiety in **15** is much more twisted with the two aromatic rings forming an angle of 37°.

Thermal, Photophysical, and Electrochemical Properties. The absorption and emission spectra of the complexes in dichloromethane solution are shown in Figures 3 and S7–S10, and the data are listed in Table 2. The complexes show strong absorption bands in the 250–300 nm region derived from ligand-centered π–π^* transitions.[17] Absorption bands in the range of 350-450 nm with lower extinction coefficients are ascribed to singlet and triplet metal-to-ligand charge-transfer (^{1}MLCT and ^{3}MLCT) states, following literature precedents[17] and the calculations of Hay.[46] Emission of the complexes is in the blue or blue-green region. The following trends in this series of complexes can be seen.

(i) Addition of the sulfone moiety results in a blue shift in emission λ_{max} relative to FIrpic of ~10 nm. The identity of the R group in $-SO_2R$ (tolyl or methyl) has little effect on the optoelectronic properties.

(ii) Exchanging a fluoro for a methoxy substituent results in a red shift of ~5 nm. Therefore, all of the monofluoro–monomethoxy complexes (**23**–**25**) have bluer emission than FIrpic, while the dimethoxy–sulfone complex **31** has a λ_{max} and emission profile comparable to FIrpic.

(iii) Addition of a mesityl group results in little change to λ_{max}, as observed previously.[33]

DOI: 10.1021/acs.inorgchem.6b01179
Inorg. Chem. 2016, 55, 8612–8627

Table 3. Electrochemical and Computed Molecular Orbital Energy Data of Iridium Complexes

complex	$E^{ox}_{1/2}$,[a] V	obs HOMO, V	complex	calcd HOMO, eV	calcd LUMO, eV	calcd HLG eV
1 FIrpic	0.89[0.92 ref16]	−5.69	**1′**	−5.49	−1.87	3.62
10	1.19	−5.99	**10′**	−6.09	−2.23	3.86
11	1.16[1.21 ref35e]	−5.96	**11′**	−5.97	−2.15	3.82
12	1.15	−5.95	**12′**	−6.01	−2.15	3.86
13	1.25	−6.05	**13′**	−6.15	−2.46	3.69
14	0.93 (irr), 1.62 (irr)[b]	−5.73	**14′**	−5.80	−2.20	3.60
15	0.94 (irr), 1.63 (irr)[b]	−5.74	**15′**	−5.61	−2.04	3.57
23	1.02	−5.82	**23′**	−5.82	−2.06	3.76
24	1.02	−5.82	**24′**	−5.74	−2.00	3.74
25	1.01	−5.81	**25′**	−5.64	−1.94	3.70
31	0.89	−5.69	**31′**	−5.53	−1.89	3.64

[a]Redox data were obtained in 0.1 M NBu_4PF_6 acetonitrile solutions and are reported vs FcH/FcH^+.[48] [b]The values reported are the cathodic peak potentials observed on the first scan.

(iv) Introducing a second sulfone group (complex **13**) results in a red shift in emission of 50 nm and a change in spectral profile, compared to FIrpic. There is literature precedent for a sulfone group inducing a red shift when introduced at the 4-position of the phenyl ring of ppy in a neutral iridium complex.[35b]

(v) Emission from the N^O bonded complexes **14** and **15** is red-shifted by ca. 10 nm relative to their pic analogues (**10** and **11**).

The photoluminescence quantum yield (PLQY) and lifetime data are stated in Table 2. The observed lifetimes (τ_P = 1.49−3.53 μs) and the spectral profiles are indicative of phosphorescence from a mixture of ligand-centered and MLCT excited states.[17,47] The PL spectra of representative complex **24** obtained at 80, 120, 160, 200, and 240 K in degassed 2-MeTHF (Figure S11) show the expected sharpening of the emission bands and a blue shift on cooling due to reduction in vibrations. This is consistent with a significant ^{3}LC contribution to the excited state.[47]

The thermal stabilities of the iridium complexes were evaluated using thermogravimetric analysis under a nitrogen atmosphere. The 5% weight loss temperatures (T_d), are above 360 °C for all complexes and are comparable to FIrpic (370 °C), suggesting the complexes should be thermally stable under device operation (Table S2).

The electrochemical properties of the complexes were examined by cyclic voltammetry (CV) in a 0.1 M NBu_4PF_6 acetonitrile solution. The observed reversible oxidation waves are assigned to the Ir(III)/Ir(IV) couple (Table 3, Figures 4 and S12). All difluoro−sulfone pic complexes (**10**−**12**) show an increase in oxidation potential of ∼0.28 V relative to that of FIrpic, indicating the sulfone group is effective at lowering the HOMO. Exchanging a fluorine for a methoxy group (**23**−**25**) results in a smaller increase in oxidation potential of ∼0.13 V relative to FIrpic, and the dimethoxy−sulfone complex **31** has an oxidation potential comparable to that of FIrpic. If the LUMO energies are assumed to be very similar in these complexes, the relative HOMO energies from their CV data are consistent with the λ_{max} values obtained from the emission spectra. The oxidation potential of **13** is +1.25 V, suggesting that addition of the second sulfone moiety lowers the HOMO; however, it must also lower the LUMO significantly, as the emission spectrum is strongly red-shifted. Complexes **14** and **15** both show two irreversible oxidation waves; if the scan is reversed before the second oxidation is reached the first oxidation wave is still irreversible. This suggests a chemical reaction takes place upon oxidation and could be attributed to the unusual connectivity around the Ir center. No additional ligand-centered oxidation waves were detected on scanning to +2.0 V for the pic complexes, and no reduction waves were observed on scanning between 0.0 and −2.0 V.

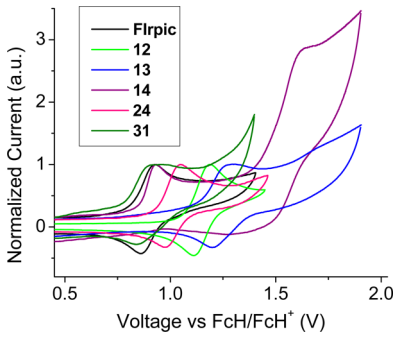

Figure 4. Cyclic voltammograms for representative complexes **1**, **12**−**14**, **24**, and **31**.

Density Functional Theory Calculations. Electronic structure calculations were performed on the 11 iridium complexes studied here (including FIrpic **1**) to explore the frontier orbitals and understand the nature of the transitions involved in the absorption and emission bands observed (Tables S3−S13). The full geometries of the iridium complexes were optimized at B3LYP/LANL2DZ:3-21G*, and the optimized geometries are denoted as **1′**, **10′**−**15′**, **23′**−**25′**, and **31′** to identify them as computed models and distinguish the predicted data from experimental data. Comparison between optimized and X-ray determined geometries reveal good agreement for the seven Ir bond distances with differences below 0.04 Å (Table S14). The complexes **10′**−**12′**, **23′**−**25′**, and **31′** have orbital contributions broadly similar to FIrpic **1′** with the HOMO on iridium and phenyl (ppy) and the LUMO on the pyridyl of the picolinate ligand (Figure 5).

The lower HOMO energies on the complexes containing the sulfonyl groups, compared to FIrpic, reflect the electron-withdrawing properties of the former. Frontier orbital energies are listed in Table 3 for direct comparison with observed CV data. The observed and computed HOMO energies are in very good agreement. The electron-donating methoxy groups in **23′**−**25′** increase the HOMO energies in **23′**−**25′** relative to **10′**−**12′**. The electron-donating effect of the four methoxy groups in **31′** cancels the electron-withdrawing effect of the two

DOI: 10.1021/acs.inorgchem.6b01179
Inorg. Chem. 2016, 55, 8612−8627

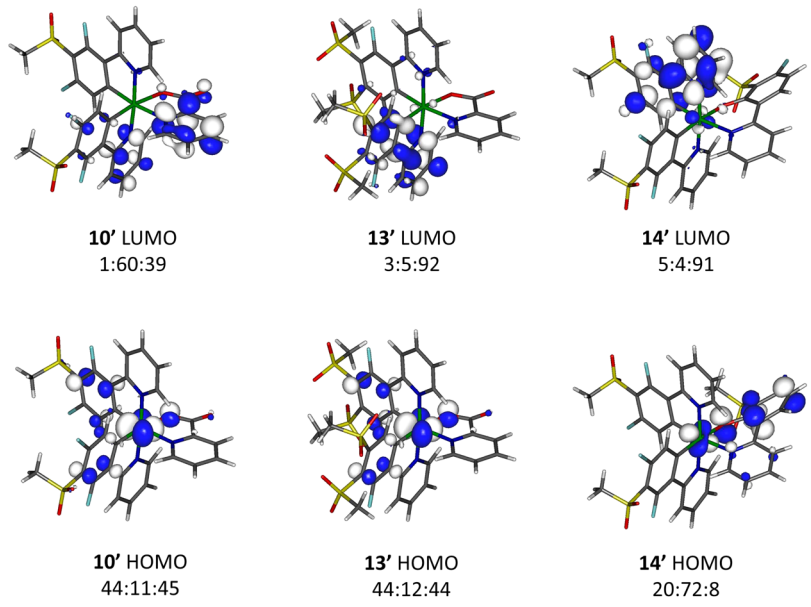

Figure 5. Frontier molecular orbitals for **10′**, **13′**, and **14′**. All contours are plotted at ±0.05 $(e/bohr^3)^{1/2}$. Ir/pic or oppy/ppy % orbital contribution ratio listed for each orbital.

sulfonyl groups; thus, **31′** has remarkably similar orbital energies and distributions to FIrpic.

The LUMOs in **10′**−**12′**, however, do have substantial contributions from the pyridyl groups of the ppy ligands, which lower their orbital energies compared to FIrpic. Nevertheless, the effect of the sulfonyl groups on the HOMO energies is larger than on the LUMO energies in complexes **10′**−**12′** and **23′**−**25′** compared to the FIrpic frontier orbitals. Therefore, the HOMO−LUMO energy gaps (HLGs) in these complexes are larger than the HLG in FIrpic, and their emissions would be more blue-shifted than FIrpic as observed experimentally.

Compound **13′** with four sulfonyl groups has a similar HOMO as the other iridium complexes discussed above, but its LUMO is located on the ppy ligand(s) not on the picolinate ligand. The different LUMO is due to the four electron-withdrawing sulfonyl groups on the ppy ligands, which would be more easily reduced than the picolinate ligand. In **13′**, the effect of the sulfonyl groups on the LUMO energy increases; thus, its HLG energy is closer to that of FIrpic than that of complexes **10′**−**12′**. While the HOMO−LUMO gap for **13** is larger than expected, the TD-DFT prediction for **13′** (see below) is 490 nm compared to **1′** at 471 nm. Thus, this supports the experimental observation that the low-energy absorption of **13** is red-shifted compared to **1**.

The HOMOs for the oppy-containing complexes, **14′** and **15′**, are located at the oppy group bonded to iridium rather than on iridium and phenyl (ppy), as is the case for the HOMOs of the other complexes here. The different HOMOs result in higher HOMO energies compared to **10′**−**12′**, and therefore **14′** and **15′** have the smallest HLG energies of all iridium complexes calculated here. The relatively high HOMO energies of **14′** and **15′** and different HOMOs to the other iridium complexes are reflected in the irreversible CV waves observed at lower oxidation potentials here. The LUMOs for **14′** and **15′** are on the ppy ligands.

TD-DFT computations were performed on the S_0-optimized geometries of **1′**, **10′**−**15′**, **23′**−**25′**, and **31′** to predict emission wavelengths of these iridium complexes. The initial excitation is assumed to give the lowest-energy singlet excited-state S_1, which in the presence of the iridium results in intersystem crossing (ISC) to form the triplet excited state T_1, and phosphorescence is observed from the $S_0 \leftarrow T_1$ process. The small Stokes shifts observed for most complexes suggest that the T_1 geometry is similar to the corresponding S_0 geometry. The reverse process $S_0 \leftarrow T_1$ is thus considered to have the same nature as the computed $S_0 \rightarrow T_1$ process with the predicted emission wavelength adjusted to take into account the Stokes shift.

Table 4 compares the predicted $S_0 \leftarrow T_1$ wavelengths with observed emission wavelengths for all iridium complexes, where the agreement is excellent except for complexes **13′**−**15′**. The emissions of complexes **13**−**15** are likely to be from different triplet excited-state geometries as shown in their subtly lower PLQYs and longer lifetimes than the other iridium complexes,

Table 4. Iridium Atom Contributions in HOMOs and Predicted Emission Wavelengths of Iridium Complexes

complex	%Ir HOMO	% Ir HOMO-1	$S_0 \leftarrow T_1$,[a] nm	$S_0 \leftarrow T_2$,[a] nm	complex	observed λ_{max}^{em},[b] nm
1′	44		471		**1**	471
10′	44		456		**10**	455
11′	42		458		**11**	457
12′	44		460		**12**	457
13′	44		490		**13**	516
14′	20[c]	45	500[c]	474	**14**	465
15′	21[c]	38	503[c]	472	**15**	468
23′	40		463		**23**	460
24′	41		467		**24**	461
25′	39		467		**25**	464
31′	40		473		**31**	474

[a]Values from TD-DFT data on S_0-optimized geometries with scaling energy factor of 0.945 based on dichloromethane at 298 K. [b]Observed highest-energy band from emission spectra (Table 2). [c]Observed emission is unlikely via ISC from S_1 to T_1, as this ISC pathway may not be promoted due to a smaller iridium contribution in the HOMO. Different triplet states with higher energies are assumed to be responsible for emissions of **14** and **15**.

DOI: 10.1021/acs.inorgchem.6b01179
Inorg. Chem. 2016, 55, 8612−8627

Table 5. Summary of Device Luminescence and Efficiency Data

complex	λ_{ELmax}, nm	brightness, cd/m^2	turn-on voltage,[a] V	EQE, %	current efficiency, cd/A	power efficiency, lm/W	CIE coordinates,[b] (x,y)
1	475	7340	6.2	5.4	12.2	5.1	(0.19, 0.38)
10	463	776	6.8	3.0	2.0	0.8	(0.19, 0.29)
11	463	2464	8.0	3.9	8.2	2.9	(0.20, 0.36)
12	465	2368	8.0	4.0	7.8	2.0	(0.18, 0.30)
23	469	1772	8.1	3.0	5.9	2.1	(0.17, 0.33)
24	469	2851	6.0	3.9	7.6	3.3	(0.17, 0.32)
25	470	2072	8.5	3.5	6.1	1.9	(0.16, 0.30)

[a]Measured at a brightness of 10 cd/m^2. [b]Measured at 12 V.

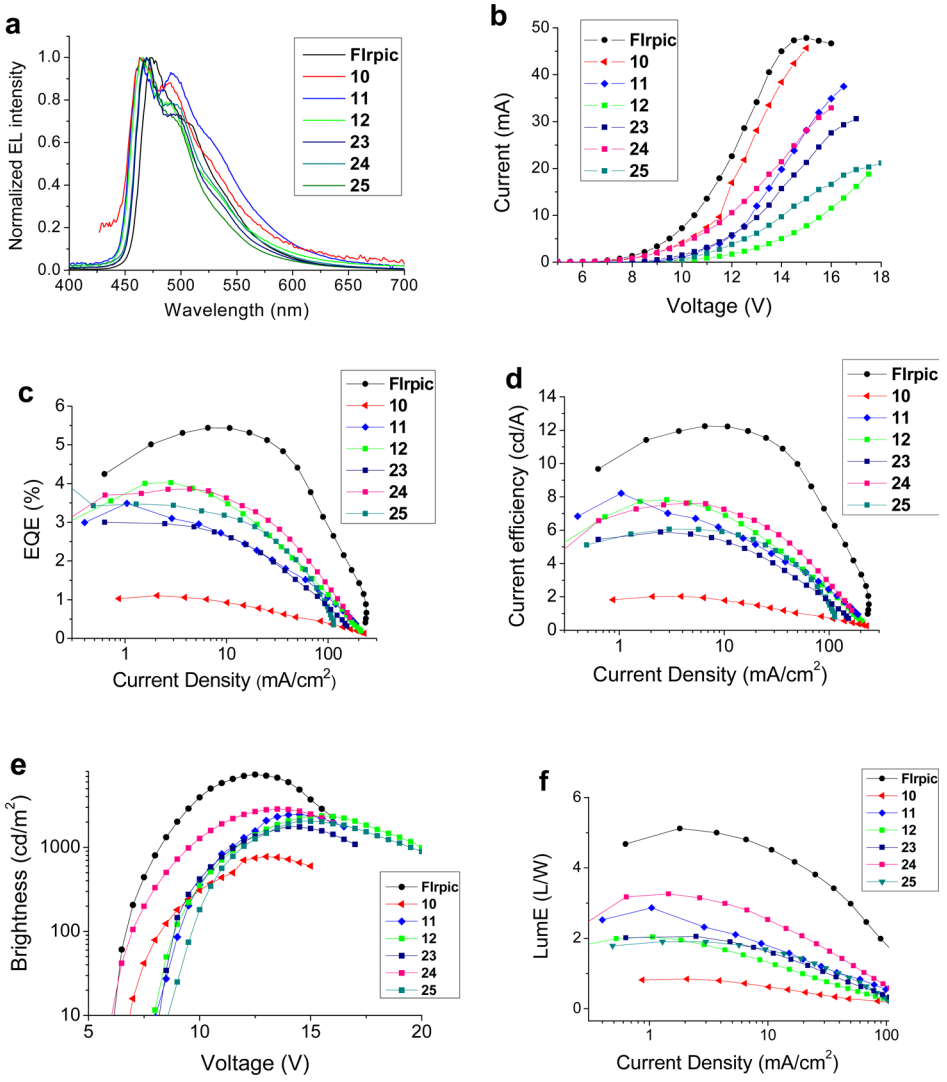

Figure 6. Electroluminescence device data. Device architecture: ITO/PEDOT:PSS (45 nm)/PVK:OXD-7(35%)/Ir complex(15%)(60 nm)/TPBi (30 nm)/LiF/Al.

1, **10**–**12**, **23**–**25**, and **31**. In the case of **13**, the larger Stokes shift observed suggests substantial rearrangement of the geometry in the T_1 excited state. The emissions from **14** and **15** may be from different triplet excited states of higher energies via ISC, as the HOMOs of **14′** and **15′** contain less iridium character (Table 4), and their S_1 excited states may not result in ISC to the predicted T_1 excited states.

The emission intensities for FIrpic and **15** were recorded at different excitation wavelengths (10 nm intervals between 380 and 430 nm, Figures S8 and S9) to examine why the predicted T_1 excited-state energies for **14** and **15** differ from the observed emission data. These measurements reveal a significant decrease in the emission intensities for **15** compared to those for FIrpic as the excitation wavelengths lengthen. The observed decrease implies a different ISC pathway in **15** compared to FIrpic and thus a different triplet excited state in **15** to the predicted T_1 state.

Optimized geometries at the T_1 excited state for **10′**, **13′**, and **14′** were performed to examine the differences in the T_1 geometries compared to their corresponding optimized S_0 geometries. From T_1 vertical energies on both S_0 and T_1 geometries, the energy differences are 0.27, 0.30, and 0.28 eV

DOI: 10.1021/acs.inorgchem.6b01179
Inorg. Chem. 2016, 55, 8612−8627

for **10′**, **13′**, and **14′**, respectively, meaning that the T_1 geometry differs (i.e., rearranges) from its S_0 geometry in **13′** more than in **10′** and **14′**. These energy values support the larger Stokes shift energy observed (Table 2) for **13** compared to the measured Stokes shift energies for all other iridium complexes.

The spin densities at the iridium atom in the optimized T_1 geometries for **10′**, **13′**, and **14′** are 0.36, 0.46, and 0.13, respectively. The low spin-density value of 0.13 for **14′** suggests that a different triplet excited state with higher energy is responsible for the phosphorescence in **14** and, by implication, **15**. The emission wavelengths in **14** and **15** would therefore be shorter than the predicted $S_0 \leftarrow T_1$ emission wavelengths, as observed experimentally. The higher spin density at the iridium atom in the optimized T_1 geometry for **13′** compared to that for **10′** may explain the less vibronic structure emission observed in **13** compared to that in **10**. An increased vibronic structure in the observed emission usually means an increased ligand contribution (and decreased metal character) to the excited state.

Phosphorescent Organic Light-Emitting Devices. PhOLEDs were fabricated using FIrpic **1** and complexes **10**−**12** and **23**−**25** as the dopant phosphor. Complexes **13**−**15** and **31** were not studied in devices as their PL spectra are red-shifted compared to the other analogues, and our focus is on obtaining blue devices. The device architecture comprised a simple single-emissive-layer, which was a blend of poly(vinylcarbazole) (PVK) as the host material, OXD-7 (an electron-transporting material), and the Ir complex to give the architecture: ITO/PEDOT:PSS (45 nm)/PVK:OXD-7(35%)/Ir complex(15%)(60 nm)/TPBi (30 nm)/LiF/Al. The emissive layer was spin-coated from chlorobenzene solution to avoid potential degradation of the complexes that can occur during thermal evaporation, especially for complexes with fluorinated ligands.[32] An additional electron-transporting layer of TPBi was incorporated adjacent to the cathode to optimize charge balance and confine excitons in the emitter layer.[49] The efficiency and luminance data of the devices are summarized in Table 5. The electroluminescence (EL) spectra for FIrpic **1** and complexes **10**−**12** and **23**−**25** are shown in Figure 6a. Several trends are apparent.

(1) For all the complexes the EL and PL spectra are similar, indicating good exciton confinement on the emissive molecules.

(2) The devices of **11**, **12**, **24**, and **25** performed better than those of **10** and **23** both in terms of external quantum efficiency (EQE) and brightness (Figure 6c,e). For **12**, **24**, and **25** this can be attributed to the presence of the mesityl group on the ppy ligands, which has been shown previously to enhance device performance.[33] The increased solubility of **11** (*p*-tolylsulfonyl substituent) compared to **10** (methylsulfonyl analogue) gave rise to better film quality for **11**, which could explain its enhanced performance.

(3) The FIrpic devices are the most efficient in this series. This can be explained by a superior trapping efficiency for the FIrpic device compared to the other complexes; the HOMO level of the PVK host is −5.8 eV, which aligns well with FIrpic (−5.69 eV, observed; −5.49 eV, calculated: Table 3). However, the HOMO levels of complexes **10**−**12** and **23**−**25** are equal to that of PVK or lower (Table 3), resulting in less efficient hole trapping. The lower efficiency for **10**−**12** and **23**−**25** is also consistent with the known trend that a rapid decline in efficiency is induced upon blue-shifting the emission color.[50]

(4) We also note that the extent of the efficiency roll-off is directly proportional to the current density and brightness for most of the devices. Efficiency roll-off in OLED devices has been comprehensively discussed.[51]

The higher efficiency, which is reproducible for complex **11** at ca. 1 mA/cm^2 (Figure 5d), is typical of some OLEDs at the device turn-on due to a slight change in material morphological defects caused by the initial current passing through the device.[52]

CONCLUSIONS

In summary, a series of heteroleptic Ir complexes [Ir(ppy)$_2$(pic)] has been synthesized with sulfonyl substituents attached to C3 of the phenyl ring of the ppy ligands. Compared to the benchmark sky-blue emitter FIrpic, the additional electron-withdrawing sulfonyl substituent results in a blue shift of the λ_{max} of PL and EL by up to ca. 12 nm as a result of the increased HOMO−LUMO gap. Replacing a fluorine atom by a methoxy group red shifts the λ_{max} of PL and EL by ca. 4−6 nm. Two complexes with an unusual 2-(2′-oxyphenyl)pyridyl ancillary ligand have been obtained by an in situ nucleophilic displacement of a fluorine substituent on a ppy ligand. (TD-)DFT calculations are in excellent agreement with the observed photophysical and electrochemical properties of the complexes. PhOLEDs have been fabricated using a selection of the complexes in a simple device architecture with a solution-processed single-emitting layer in the configuration ITO/PEDOT:PSS/PVK:OXD-7(35%)/Ir complex(15%)/TPBi/LiF/Al. The EL data confirm the potential of the new complexes to serve as blue dopants in functional devices with a notably lower CIE C_y coordinate compared to FIrpic. The work provides further examples where the efficiency of blue PhOLEDs is enhanced by the presence of a mesityl substituent on the pyridyl ring of the ppy ligands.

EXPERIMENTAL SECTION

Materials, Synthesis, and Characterization. All commercially available chemicals were used without further purification. Reactions requiring an inert atmosphere were performed under a blanket of argon gas, which was dried over a phosphorus pentoxide column. Anhydrous solvents were dried through an HPLC column on an Innovative Technology Inc. solvent-purification system. Column chromatography was performed using 40−60 μm mesh silica gel. Analytical thin-layer chromatography (TLC) was performed on plates precoated with silica gel (Merck, silica gel 60F$_{254}$) and visualized using UV light (254, 315, 365 nm). NMR spectra (Figures S13−S34) were recorded on Bruker Avance 400 MHz, Varian Mercury 200 and 400 MHz, Varian Inova 500 MHz, or Varian VNMRS 600 and 700 MHz spectrometers. Chemical shifts are referenced to tetramethylsilane [Si(CH$_3$)$_4$] at 0.00 ppm. Melting points were determined in open-ended capillaries using a Stuart Scientific SMP3 melting point apparatus at a ramping rate of 1 °C/min. They are recorded to the nearest 0.1 °C. Electrospray ionization (ESI) and matrix-assisted laser desorption/ionization mass spectra were recorded on a Thermo-Finnigan LTQ FT (7.0 T magnet) spectrometer. Atmospheric solids analysis probe mass spectra were recorded on a Waters Xevo QTOF spectrometer. Gas chromatography mass spectrometry (GCMS) spectra were recorded on a Thermo-Finnigan Trace GCMS (EI and CI ion sources). Elemental analyses were obtained on an Exeter Analytical Inc. CE-440 elemental analyzer. HPLC was performed on

DOI: 10.1021/acs.inorgchem.6b01179
Inorg. Chem. 2016, 55, 8612−8627

an analytical/semiprep Varian LC system equipped with UV−vis and ES^+ mass detectors.

Solution Electrochemistry and Photophysics. Cyclic voltammetry experiments were recorded using a BAS CV50W electrochemical analyzer fitted with a three-electrode system consisting of a Pt disk (Ø = 1.8 mm) as the working electrode, a Pt wire as an auxiliary electrode, and a $Ag/AgNO_3$ (0.1 M[NEt_4][ClO_4] in CH_3CN) system as the reference electrode. Experiments were conducted in dry acetonitrile solution with *n*-Bu_4NPF_6 (0.1 M) as the supporting electrolyte at a scan rate of 100 mV/s. The reference electrode was assumed to be stable and was referenced externally to ferrocene (Cp_2Fe) and decamethylferrocene (Cp^*_2Fe), which displayed potentials ($E_{1/2}$) of −0.41 V and +0.10 V, respectively, versus $Ag/AgNO_3$ under these conditions. It was not possible to use Cp_2Fe or Cp^*_2Fe as an internal reference because their addition to the solutions of the complexes resulted in a distortion of the redox waves of the complexes.

Solution-state photophysical data were obtained using freshly prepared solutions of the complexes in dichloromethane (DCM). Emission and lifetime measurements used thoroughly degassed solutions achieved by three freeze−pump−thaw cycles and quartz cuvettes with a path length of 1 cm. The solutions had absorbance below 0.10 to minimize inner filter effects. UV−vis absorption measurements were recorded using a Unicam UV2−100 spectrometer operated with Unicam Vision(ver. 3.50) software. Baseline correction was achieved by reference to pure solvent in the same cuvette. Absorption measurements were obtained using quartz cuvettes with a path length of 2 cm.

Excitation and emission spectra were recorded on a Jobin−Yvon−Horiba SpexFluoromax 3 Spectrometer. Solutions of the complexes in degassed DCM [$<1 \times 10^{-5}$ M] were used for decay measurements. Samples were excited with a pulsed nitrogen laser emitting at 337.1 nm. Emission was focused onto a spectrograph and detected on a sensitive gated iCCD camera (Stanford Computer Optics) with sub-nanosecond resolution. Solution PLQYs were recorded in degassed solvent and determined using the relative method, with $Ir(ppy)_3$ (Φ_{PL} = 0.46 in degassed dichloromethane, determined in house, vs Φ_{PL} = 0.546 in 0.5 M H_2SO_4) as the reference. The PLQYs were calculated according to the following equation:

$$\Phi_x = \Phi_{ref}\frac{Grad_x}{Grad_{ref}}\cdot\left(\frac{\eta_x}{\eta_{ref}}\right)^2$$

where subscripts "x" and "ref" denote the material being measured and the reference, respectively. Φ represents the PLQY, Grad is the gradient from the plot of integrated fluorescence intensity versus absorbance, and η is the refractive index of the solvent.

Computational Studies. All calculations were performed with the Gaussian 09 package.[53] All optimized S_0 geometries were performed using B3LYP[54] with the pseudopotential (LANL2DZ)[55] for iridium and 3-21G* basis set for all other atoms.[56] This model chemistry was selected on the basis of related computational studies on [$Ir(ppy)_2Cl]_2$[57] and $Ir(ppy)_3$.[58] All S_0-optimized geometries of the most stable conformers were true minima based on no imaginary frequencies found. Electronic structure and TD-DFT calculations were also from the optimized geometries at B3LYP/LANL2DZ:3-21G*. The MO diagrams and orbital contributions were generated with the aid of Gabedit[59] and GaussSum[60] packages, respectively. The TD-DFT method does not include spin−orbit couplings; thus, no oscillation strengths for the triplet excited states are given and also does not compute mixed singlet−triplet excited states. Optimized triplet excited-state (T_1) geometries were also performed on **10′**, **13′**, and **14′** to examine significant changes between their S_0 and T_1 geometries to explain the differences in observed and computed emission values for **13** and **14**. Optimized triplet excited-state (T_1) geometries by TD-DFT can be considered unreliable,[58] so our interpretations are based on the assumption that these geometries are accurate.

Phosphorescent Organic Light-Emitting Devices. PhOLEDs were fabricated on indium tin oxide (ITO)-coated glass substrates of thickness 125 nm and possessing a sheet resistance of 15 Ω/x. Poly(3,4-ethylenedioxythiophene) doped with high work function hole injection layer poly(styrenesulfonic acid) (PEDOT:PSS) (HIL1.3), from CLEVIOS, was spin-coated at 2500 rpm for 60 s to produce an ∼50 nm thick hole-injecting/transporting layer (HTL). The PEDOT:PSS layer was annealed at ca. 200 °C for 5 min to remove any residual water. A chlorobenzene solution of 25 mg/mL of poly(vinylcarbazole) (PVK; Mw = 90 000) was doped with 30% w/w of (1,3-phenylene)bis[5-(4-*tert*-butylphenyl)-1,3,4-oxadiazole] (OXD-7). Blended devices were made by mixing 15% w/w of the Ir complexes. The prepared mixtures were filtered with a 0.45 μm pore filter and spin-coated at 2500 rpm for 1 min on the top of the PEDOT:PSS layer and baked for 10 min at 120 °C. Each sample was shadow masked to produce four identical devices of area 4 × 5 mm; the samples were then introduced into a nitrogen glovebox, where 30 nm of 2,2′,2″-(1,3,5-benzenetriyl)tris-[1-phenyl-1*H*-benzimidazole] (TPBi) was evaporated as an electron injection/hole blocking layer at a rate of ∼1 Å/s under vacuum at a pressure of ca. 1×10^{-6} Torr, followed by 0.8 nm LiF and a 100 nm capping layer of aluminum under the same evaporation conditions. Therefore, the device configuration for all complexes was: ITO/PEDOT:PSS (50 nm)/PVK:OXD-7 (35%)/Ir complex (15%)/TPBi (30 nm)/LiF(0.8 nm)/Al(100 nm). All samples were encapsulated inside a glovebox using DELO UV cured epoxy (KATIOBOND) and capped with a 1.2 × 1.2 cm microscope glass slide then exposed to UV light for 3 min. Current−voltage data, device efficiency, brightness, and electroluminescence spectra were measured in a calibrated Labsphere LMS-100 integrating sphere. A home-written NI LabVIEW program was used to control an Agilent 6632B DC power supply, and the emission properties of the device were measured using an Ocean Optics USB4000 CCD fiber optic spectrometer. Thicknesses of the various layers in the device were measured with a J. A. Woolam VASE Ellipsometer using thin films that had been spin-coated on Si/SiO_2 substrates under the same conditions as the device films.

General Procedure for ortho Lithation Followed by Iodination. ^{n}BuLi (1.2 equiv) was added to a stirred solution of *N*,*N*-diisopropylamine (DIPA; 1.3 equiv) in dry tetrahydrofuran (THF) at 0 °C, and the solution was stirred for 30 min. The temperature was then lowered to −78 °C, and a solution of the substrate (1 equiv) in dry THF was added in portions via cannula; the mixture was stirred for a further 1 h. A solution of I_2 (1.1−1.3 equiv) in dry THF was added to the flask dropwise. The solution was stirred at −78 °C and allowed to warm to room temperature (RT) overnight. The solution was then quenched with an aqueous solution of NaS_2O_3 to remove unreacted LDA and I_2. The solution was then extracted with DCM (3 × 75 mL), and the organic phases were combined, dried over $MgSO_4$, and filtered; the solvent was reduced in vacuo. The residue was passed through a silica plug (eluent: DCM/ethyl acetate) to remove baseline impurities revealed by TLC. The solvent was removed, and the crude product was either triturated with cold hexane or purified by column chromatography, to remove any unreacted starting material. The product was then dried on a high vacuum line to leave the pure product.

General Procedure for Sulfone Synthesis. The iodo compound (1 equiv), the sodium sulfinate derivative (1.6 equiv) and CuI (1.5 equiv) were dissolved in dry dimethylformamide (DMF) and stirred under argon. The mixture was heated at 110 °C overnight. The mixture was cooled to RT, and water (20 mL) and DCM (20 mL) were added. The solid was filtered off and washed with more DCM. The organic layer was separated and dried over $MgSO_4$, and the solvent was removed in vacuo. The residue was purified by column chromatography to give pure product, unless otherwise specified. This is in accordance with the method described in the literature.[38]

General Procedure for Synthesis of Iridium pic Complexes. Method A. $IrCl_3{\cdot}3H_2O$ (1 equiv) was added to a stirred solution of the cyclometalating ligand (2.1−2.2 equiv) in 2-ethoxyethanol. The mixture was heated to reflux at 130 °C under argon overnight. The mixture was then left to cool, and the solvent was removed in vacuo. The yellow solid, presumed to be the intermediate bis(μ-Cl) dimer complex, was washed with cold hexane to remove any free ligand and dried. Where possible, the bis(μ-Cl) dimer was characterized by ^{1}H

DOI: 10.1021/acs.inorgchem.6b01179
Inorg. Chem. 2016, 55, 8612−8627

NMR and mass spectrometry, although attempted purification usually led to decomposition. The dimer was then suspended in 2-ethoxyethanol, and picolinic acid (<3 equiv) was added. The mixture was stirred and heated to reflux (130 °C) under argon overnight. The mixture was allowed to cool to RT, and the solvent was removed. The product was then purified by column chromatography to give pure product, unless otherwise specified.

Method B. The reaction was conducted via a one-pot method, and the intermediate bis(μ-Cl) dimer was not isolated.

Synthesis of Ligands and Complexes. *2-(2,4-Difluoro-3-iodophenyl)-4-(2,4,6-trimethylphenyl)pyridine (**5**).* The reaction followed the general procedure for lithiation/iodination using ^{n}BuLi (3.69 mL, 2.5 M), DIPA (1.40 mL, 9.99 mmol), 2-(2,4-difluorophenyl)-4-(2,4,6-trimethylphenyl)pyridine **3**[33a] (2.38 g, 7.68 mmol), I_2 (2.14 g, 8.43 mmol), and THF (45 mL). The mixture was purified using a Biotage Isolera One purification system to give **5** as a white semisolid (2.50 g, 75%); δ_H (400 MHz, $CDCl_3$, Me_4Si) 8.77 (1H, dd, *J* 5.0 0.9), 8.07 (1H, td, *J* 8.7 6.4), 7.59 (1H, dt, *J* 2.4 1.3), 7.12 (1H, dd, *J* 4.9 1.5), 7.05 (1H, ddd, *J* 8.6 6.9 1.5), 6.98 (2H, s), 2.35 (3H, s), 2.06 (6H, s); δ_F (376 MHz, $CDCl_3$, Me_4Si) −90.98 (1F, q, *J* 5.7), −93.59, −93.67 (1F, m); δ_C (101 MHz, $CDCl_3$, Me_4Si) δ_C (101 MHz, $CDCl_3$, Me_4Si) 161.85 (dd, *J* 249.4 5.4), 158.83 (dd, *J* 250.2, 5.9), 152.15 (d, *J* 3.4), 150.31, 150.07, 137.75, 136.13, 135.20, 132.31 (dd, *J* 9.2, 4.2), 128.50, 125.50 (d, *J* 9.4), 124.46 (dd, *J* 14.4, 3.7), 123.96, 111.94 (d, *J* 3.7), 111.71 (d, *J* 3.7), 72.01 (dd, *J* 30.9, 29.3), 21.16, 20.71; HRMS (FTMS+ESI): calcd for $[C_{20}H_{16}NF_2I+H]^+$: 436.0374. Found: 436.0378.

*2-[2,4-Difluoro-3-(methanesulfonyl)phenyl]pyridine (**6**).* Using the general procedure for sulfone synthesis the following reagents were used: 2-(2,4-difluoro-3-iodophenyl)pyridine **4**[35e] (1.00 g, 3.15 mmol), sodium methanesulfinate (0.515 g, 5.05 mmol), copper iodide (0.90 g, 4.73 mmol), and DMF (3 mL). Purification by column chromatography (4% EtOAc in DCM, increased to 20% EtOAc in DCM) gave a product that was recrystallized from a mixture of hexane and DCM to give **6** as a white solid (0.133, 15%); mp 95.2−97.0 °C; δ_H (400 MHz; $CDCl_3$; Me_4Si) 8.72 (1H, dt, *J* 4.8 1.4), 8.27 (1H, td, 8.6 6.0), 7.71−7.87 (2H, m), 7.32 (1H, ddd, *J* 6.7 4.8 2.1), 7.18 (1H, td, 9.2 1.6), 3.34 (3H, s); δ_F (376 MHz, $CDCl_3$, Me_4Si) −106.14 (1F, dd, *J* 9.3 6.2), −111.50 (1F, d, *J* 8.3); δ_C (101 MHz, $CDCl_3$, Me_4Si) 159.86 (dd, *J* 262.6 4.0), 157.50 (dd, *J* 262.6 3.9), 150.89, 150.18, 137.32 (dd, *J* 10.9 5.8), 136.90, 125.80 (dd, *J* 13.7 4.1), 124.63 (d, *J* 9.5), 123.42, 118.55 (dd, *J* 17.3 15.5), 113.80 (dd, *J* 23.1 4.0), 45.88 (t, *J* 2.4); HRMS (FTMS+ESI): calcd for $[C_{12}H_9F_2NO_2S+H]^+$: 270.03948. Found: 270.03938.

*2-(2,4-Difluoro-3-[(4-methylbenzene)sulfonyl]phenyl)pyridine (**7**).* 2-(2,4-Difluoro-3-iodophenyl)pyridine **4** (2.17 g, 6.84 mmol), sodium *p*-toluenesulfinate (1.95 g, 10.94 mmol), and copper iodide (1.95 g, 10.23 mmol) were dissolved in DMF (10 mL) and stirred under argon. The mixture was heated at 110 °C overnight. Column chromatography (4% EtOAc in DCM) gave a product that was recrystallized from a hexane/DCM mixture to give **7** as white crystals (0.62 g, 26%); 99.5−100.9 °C; δ_H (400 MHz; $CDCl_3$; Me_4Si) 8.67−8.71 (1H, m), 8.18 (1H, td, *J* 8.6, 6.0), 7.98 (2H, d, *J* 8.1), 7.70−7.81 (2H, m), 7.34 (2H, d, *J* 8.1) 7.29 (1H, ddd, *J* 6.7, 4.8, 2.1), 7.10 (1H, td, *J* 9.2, 1.6), 2.42 (3H, s); δ_F (376 MHz; $CDCl_3$; Me_4Si) −106.13 (1F, dd, *J* 9.3, 6.0), −111.44 (1F, d, *J* 8.1); δ_C (176 MHz; $CDCl_3$; Me_4Si) 159.9 (dd, *J* 263.1, 3.8), 157.4 (dd, *J* 263.1, 3.5), 151.2, 150.1, 145.4, 139.1, 137.0 (dd, *J* 10.9, 5.7), 136.8, 130.0, 128.0, 125.6 (dd, *J* 13.6, 4.3), 124.8, 124.7, 123.3, 119.9 (t, *J* 15.9), 113.7 (dd, *J* 23.3, 3.8), 21.8; HRMS (FTMS+ESI): calcd for $[C_{18}H_{13}F_2NO_3S+H]^+$: 346.0713. Found: 346.0692. These data are consistent with the literature data for **7** prepared by a different route.[35e]

*2-(2,4-Difluoro-3-[methanesulfonyl]phenyl)-4-(2,4,6-trimethylphenyl)pyridine (**8**).* The reaction followed the general procedure for sulfone synthesis using 2-(2,4-difluoro-3-iodophenyl)-4-(2,4,6-trimethylphenyl)pyridine **5** (657 mg, 1.51 mmol), sodium methanesulfinate (247 mg, 2.42 mmol), CuI (431 mg, 2.26 mmol), and DMF (3 mL). The product was purified by column chromatography (2.5% EtOAc in DCM, increased to 10% v/v) to give **8** as an off-white solid (130 mg, 22%); mp 74.6−77.5 °C; δ_H (400 MHz; $CDCl_3$; Me_4Si) 8.77 (1H, d, *J* 5.0), 8.36 (1H, td, *J* 8.6 6.0), 7.58−7.64 (1H, m), 7.21 (1H, td, *J* 9.0, 1.5), 7.13−7.17 (1H, m), 6.96 (2H, d, *J* 1.1), 3.33 (3H, s), 2.33 (3H, s), 2.03 (6H, s); δ_C (101 MHz, $CDCl_3$, Me_4Si) 159.81 (dd, *J* 262.6, 4.0), 157.46 (dd, *J* 262.0, 4.0), 156.18 (d, *J* 3.9), 151.00 (d, *J* 2.1), 150.59 (s), 150.25 (s), 137.83 (s), 137.31 (dd, *J* 10.8, 5.7), 135.79 (s), 135.03 (s), 128.47 (s), 125.96−125.56 (m), 124.43 (s), 118.54 (dd, *J* 17.6, 15.5), 113.77 (dd, *J* 23.1, 3.9), 45.79 (t, *J* 2.4), 21.09 (s), 20.64 (s); δ_F (376 MHz, $CDCl_3$, Me_4Si) −106.14 (1F, dd, *J* 10.2, 8.6), −111.40 (1F, d, *J* 11.0); HRMS (FTMS+ESI): calcd for $[C_{21}H_{19}F_2NO_2S+H]^+$: 388.1183. Found: 388.1170.

*2-(2-Fluoro-3,4-di[methanesulfonyl]phenyl)pyridine (**9**).* The reaction followed the general procedure for sulfone synthesis using 2-(2,4-difluoro-3-iodophenyl)pyridine **4** (which had not been rigorously purified and was presumed to be contaminated with iodine; 1.00 g, 3.15 mmol), sodium methanesulfinate (0.515 g, 5.05 mmol), CuI (0.90 g, 4.73 mmol), and DMF (3 mL). The reaction was worked up as described in the general procedure, and the crude product mixture was subjected to column chromatography (1:2 EtOAc in DCM, increased to 1:1 v/v to elute the final fraction). ^{1}H NMR analysis revealed a mixture of products. The mixture was columned for a second time (10% EtOAc in DCM) to give two white solid products, 2-(2,4-difluoro-3-[methanesulfonyl]phenyl)pyridine **6** (135 mg, 16%; identical with the sample above) and 2-(2-fluoro-3,4-di-[methanesulfonyl]phenyl)pyridine **9** (115 mg, 11%); mp 194.0−198.1 °C; δ_H (400 MHz; $CDCl_3$; Me_4Si) 8.78 (1H, d, *J* 4.7), 8.46 (1H, dd, *J* 8.4 6.9), 8.28 (1H, dd, *J* 8.3 1.1), 7.83−7.91 (2H, m), 7.39 (1H, td, J 4.8, 2.4), 3.58 (3H, s), 3.49 (3H, s); δ_F (376 MHz, $CDCl_3$, Me_4Si) −106.57 (1F, d, *J* 6.9); δ_c (101 MHz, $CDCl_3$, Me_4Si) 159.10 (d, *J* 265.4), 150.49, 150.13 (d, *J* 1.8), 143.03, 137.01, 136.64 (d, *J* 5.2), 135.16 (d, *J* 15.3), 129.59 (d, *J* 14.7), 128.15 (d, *J* 3.5), 125.20 (d, *J* 9.8), 124.34, 46.27, 45.28; HRMS (FTMS+ESI): calcd for $[C_{13}H_{12}FNO_4S_2+H]^+$: 330.0270. Found: 330.0273.

*Iridium Complex **10**.* The reaction followed the general procedure for the synthesis of iridium pic complexes, Method A, using $IrCl_3 \cdot 3H_2O$ (107 mg, 0.30 mmol), 2-(2,4-difluoro-3-[methanesulfonyl]-phenyl)pyridine **6** (180 mg, 0.67 mmol), picolinic acid (154 mg, 1.25 mmol), and 2-ethoxyethanol (10 mL). Attempted purification of a small portion of the intermediate μ-dichloro dimer resulted in rapid decomposition under ambient conditions, so no characterization data were obtained. Purification by column chromatography (DCM/acetone, 1:1) gave **10** as a yellow solid (190 mg, 85%); Anal. Calcd for $C_{30}H_{20}F_4IrN_3O_6S_2$: C, 42.35; H, 2.37; N, 4.94. Found: C, 42.17; H, 2.23; N, 4.88%; δ_H (700 MHz; $CDCl_3$; Me_4Si) 8.75 (1H, dt, *J* 5.8, 1.3, H_{D6}), 8.39 (1H, d, *J* 8.4, H_{B3}), 8.35 (1H, d, *J* 7.8, H_{A3}), 8.34 (1H, d, *J* 8.8, H_{D3}), 8.04 (1H, td, *J* 7.8, 1.6, H_{A4}), 7.93 (1H, td, *J* 6.4, 1.6, H_{B4}), 7.91 (1H, td, *J* 6.4, 1.7, H_{D4}), 7.75 (1H, dt, *J* 5.1, 1.4, H_{A6}), 7.54 (1H, ddd, *J* 7.8, 5.4, 1.5, H_{A5}), 7.45 (1H, dd, *J* 5.7, 1.4, H_{B6}), 7.35 (1H, ddd, *J* 7.3, 5.8, 1.4, H_{D5}), 7.14 (1H, ddd, *J* 7.4, 5.8, 1.4, H_{B5}), 5.97 (1H, d, *J* 10.0, H_{E6}), 5.73 (1H, d, *J* 10.1, H_{C6}), 3.27 (3H, s, H_{E7}), 3.21 (3H, s, H_{C7}); δ_F (376 MHz, $CDCl_3$, Me_4Si) −105.12 (1F, d, 9.8), −106.30 (1F, d, 10.0), −109.57 (1F, s), −110.28 (1F, s); δ_C (176 MHz; $CDCl_3$; Me_4Si) 172.36 (s, C_{A7}), 164.19 (d, *J* 6.8,C_{B2}), 162.97 (d, J 6.4, C_{D2}), 161.34 (d, *J* 8.1, C_{C2}), 160.60 (d, *J* 8.5, C_{E2}), 159.66 (dd, *J* 268.2, 2.82, C_{E5}), 159.19 (dd, *J* 266.4, 3.0, C_{C5}), 157.54 (dd, *J* 271.1, 3.50, C_{E3}), 157.33 (dd, *J* 270.0, 4.5, C_{C3}), 151.11 (s, C_{A2}), 148.89 (s, C_{D6}), 148.41 (s, C_{B6}), 148.32 (s, C_{A6}), 139.58 (s, $C_{B/D4}$), 139.57 (s, $C_{B/D4}$), 139.46 (s, C_{A4}), 130.10 (m, C_{C1}), 129.92 (m, C_{E1}), 129.18 (s, $C_{A3/5}$), 129.11

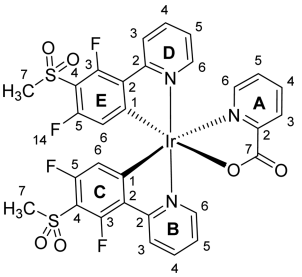

DOI: 10.1021/acs.inorgchem.6b01179
Inorg. Chem. 2016, 55, 8612−8627

(s, $C_{A3/5}$), 124.49 (d, *J* 21.8, C_{B3}), 124.21 (s, C_{D5}), 124.14 (s, C_{B5}), 124.00 (d, *J* 20.6, C_{D3}), 116.64 (d, *J* 19.3, C_{E6}), 116.45 (d, *J* 19.1, C_{C6}), 111.83 (t, *J* 16.6, C_{C4}), 111.22 (t, *J* 16.5, C_{E4}), 45.94 (s, $C_{C7/E7}$), 45.90 (s, $C_{C7/E7}$); HRMS (FTMS+ESI): calcd for $[C_{30}H_{20}F_4N_3O_6S_2{}^{191}Ir+H]^+$: 850.0414. Found: 850.0439. Crystals for X-ray analysis were grown by slow evaporation of a DCM solution of **10**.

Iridium Complex ***11***. The reaction followed the general procedure for synthesis of iridium pic complexes, Method A, using $IrCl_3{\cdot}3H_2O$ (278 mg, 0.79 mmol), 2-(2,4-difluoro-3-[(4-methylbenzene)sulfonyl]-phenyl)pyridine **7** (600 mg, 1.78 mmol), and 2-ethoxyethanol (20 mL) to give the intermediate μ-dichloro dimer as a yellow solid (700 mg, 96%); δ_H (400 MHz; $CDCl_3$; Me_4Si) 8.91 (4H, dd, *J* 6.2, 1.4), 8.35 (4H, d, *J* 8.5), 7.88−7.94 (4H, m), 7.83 (8H, d, *J* 8.1), 7.24 (8H, d, *J* 8.5), 6.87 (4H, ddd, *J* 7.4, 5.8, 1.4), 5.24 (4H, d, *J* 10.6), 2.36 (12H, s); δ_F (376 MHz; $CDCl_3$; Me_4Si) −105.27 (4F, d, *J* 10.4), −109.88 (4F, s); HRMS (FTMS+ESI): calcd for $[C_{72}H_{48}Cl_2F_8{}^{191}Ir_2N_4O_8S_4+Na_2]^{2+}$: 939.0320. Found: 939.0303. The reaction proceeded as described in the general Method A using Ir dimer (500 mg, 0.27 mmol), picolinic acid (336 mg, 2.73 mmol), and 2-ethoxyethanol (10 mL). The reaction was worked up as previously described, and the product was purified by column chromatography (THF/DCM, 3:7 v/v), followed by recrystallization from DCM/hexane to give **11** as a yellow solid (421 mg, 77%). Anal. Calcd for $C_{42}H_{28}F_4IrN_3O_6S_2$: C 50.29; H 2.81; N 4.19. Found: C 50.03; H 2.96; N 4.01%; δ_H (400 MHz; acetone-d_6, Me_4Si) 8.65 (1H, dt, *J* 5.7, 1.1), 8.37 (2H, t, *J* 8.3), 8.19−8.07 (4H, m), 7.94 (1H, d, *J* 5.2), 7.87 (4H, t, *J* 7.6), 7.80 (1H, d, *J* 5.8), 7.62 (1H, ddd, *J* 6.6, 5.4, 2.6), 7.55 (1H, ddd, *J* 7.4, 5.8, 1.4), 7.43−7.34 (5H, m), 6.01 (1H, d, *J* 10.7), 5.70 (1H, d, *J* 10.6), 2.41 (3H, s), 2.40 (3H, s); δ_F (376 MHz; acetone-d_6; Me_4Si) −107.87 (1F, dd, *J* 10.7, 4.1), −108.61 (1F, dd, *J* 10.6, 3.6), −110.89 (1F, s), −111.59 (1F, s); HRMS (FTMS+ESI): calcd for $[C_{42}H_{28}O_6N_3F_4{}^{191}IrS_2+Na]^+$: 1026.0883. Found: 1026.0870. These data are consistent with the literature data for **11** prepared by a different route.[35e] Crystals for X-ray analysis were grown by slow evaporation of a DCM/hexane solution of **11**.

Iridium Complex ***12***. The reaction followed the general procedure for synthesis of iridium pic complexes, Method A, using $IrCl_3{\cdot}3H_2O$ (40 mg, 0.11 mmol), 2-(2,4-difluoro-3-[methanesulfonyl]phenyl)-4-(2,4,6-trimethylphenyl)pyridine **8** (90 mg, 0.232 mmol), and 2-ethoxyethanol (6 mL) to give the intermediate μ-dichloro dimer as a yellow solid. The NMR spectra were consistent with the dimer structure: δ_H (400 MHz; $CDCl_3$; Me_4Si) 9.52 (4H, d, *J* 5.9), 8.23 (4H, s), 6.97−7.05 (12H, m), 5.34 (4H, d, *J* 10.8), 3.18 (3H, s), 2.40 (3H, s), 2.11 (3H, s), 2.07 (3H, s); δ_F (376 MHz, $CDCl_3$, Me_4Si) −105.73 (4F, d, *J* 12.0), −110.17 (4F, s). The reaction was continued as described in the general Method A using Ir dimer, picolinic acid (90 mg, 0.731 mmol), and 2-ethoxyethanol (6 mL). The product was purified by column chromatography (EtOAc/DCM 3:7 v/v) to afford Ir complex **12** as a yellow solid (105 mg, 85%); Anal. Calcd for $C_{48}H_{40}F_4IrN_3O_6S_2{\cdot}0.5CH_2Cl_2$: C, 51.57; H, 3.66; N, 3.72. Found: C, 51.32; H, 3.62; N, 3.69%; δ_H (400 MHz; $CDCl_3$; Me_4Si) 8.82 (1H, dd, *J* 6.0 0.7), 8.40−8.48 (1H, m), 8.21 (1H, t, *J* 1.7), 8.15 (1H, t, *J* 1.7), 8.09 (1H, td, *J* 7.8 1.6), 7.89 (1H, ddd, *J* 5.4 1.6 0.8), 7.60 (1H, ddd, *J* 7.8 5.3 1.5), 7.50 (1H, dd, *J* 6.0 0.7), 7.21 (1H, dd, *J* 5.9 1.7), 6.95−7.04 (5H, m), 5.94 (1H, d, *J* 10.3), 5.73 (1H, d, *J* 10.4), 3.25 (3H, s), 3.20 (3H, s), 2.35 (6H, s), 2.12 (3H, s), 2.09 (6H, s), 1.96 (3H, s); δ_F (376 MHz, $CDCl_3$, Me_4Si) −105.58 (1F, dd, *J* 10.9 3.5), −106.77 (1F, dd, *J* 11.4 3.3), −109.82 (1F, d, *J* 4.1), −110.61; HRMS (FTMS+ESI): calcd for $[C_{48}H_{40}F_4N_3O_6S_2{}^{191}Ir + H]^+$: 1086.1979. Found: 1086.1978. Crystals for X-ray analysis were grown by slow evaporation of a DCM/hexane solution of **12**.

Iridium Complex ***13***. The reaction followed the general procedure for synthesis of iridium pic complexes, Method A, using $IrCl_3{\cdot}3H_2O$ (94 mg, 0.27 mmol), 2-(2-fluoro-3,4-bis(methylsulfonyl)phenyl)-pyridine **9** (194 mg, 0.59 mmol), and 2-ethoxyethanol (8 mL) to give an orange-yellow solid presumed to be the bis(μ-Cl) dimer, which was used without further purification. Because of its very poor solubility NMR data could not be obtained. The reaction was continued as described in the general Method A using picolinic acid (245 mg, 1.99 mmol) and 2-ethoxyethanol (8 mL). The product was purified by column chromatography (DCM/acetone 1:1 v/v) to give **13** as a yellow solid (208 mg, 80%); Anal. Calcd for $C_{32}H_{26}F_2IrN_3O_{10}S_4$: C, 39.58; H, 2.70; N, 4.33. Found: C, 39.42; H, 2.61; N, 4.42%; δ_H (400 MHz; $CDCl_3$; Me_4Si); 8.85 (1H, d, *J* 5.2), 8.52 (1H, d, *J* 8.6), 8.48 (1H, d, *J* 8.6), 8.36 (1H, d, *J* 7.5), 7.97−8.10 (3H, m), 7.70 (1H, d, *J* 5.2), 7.62 (1H, d, *J* 6.0), 7.57 (1H, t, *J* 6.4), 7.49 (1H, t, *J* 6.4), 7.29 (1H, t, *J* 6.6), 7.14 (1H, s), 6.83 (1H, s), 3.43 (3H, s), 3.41 (3H, s), 3.37 (3H, s), 3.36 (3H, s); δ_F (376 MHz, $CDCl_3$, Me_4Si) −105.51 (1F, s), −106.32 (1F, s); HRMS (FTMS+ESI): calcd for $[C_{32}H_{26}F_2N_3O_{10}S_4{}^{191}Ir+H]^+$: 970.0153. Found: 970.0177. Crystals for X-ray analysis were grown by slow evaporation of a DCM/acetonitrile solution of **13**.

Iridium Complex ***14***. $IrCl_3{\cdot}3H_2O$ (69 mg, 0.20 mmol) was added to a stirred solution of 2-(2,4-difluoro-3-[methanesulfonyl]phenyl)-

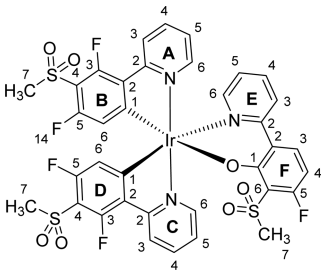

pyridine **6** (116 mg, 0.67 mmol) in 2-ethoxyethanol (8 mL). The mixture was heated to reflux at 130 °C under argon overnight. The mixture was then left to cool, and the solvent was removed in vacuo to give a yellow solid, presumed to be the bis(μ-Cl) dimer, which was used without further purification. The dimer was dissolved in ethylene glycol (8 mL), and 2-(2,4-difluoro-3-[methanesulfonyl]phenyl)-pyridine **6** (58 mg, 0.22 mmol), NEt_3 (0.1 mL), and acetylacetone (0.1 mL) were added. The mixture was stirred under argon and heated to reflux at 190 °C overnight. The mixture was then left to cool. DCM (25 mL) and water (25 mL) were added, and the organic layer was separated and washed with water (2 × 60 mL) to remove most of the ethylene glycol. The solvent was removed in vacuo to leave a brown liquid residue, which was washed with water (5 mL) to remove any residual ethylene glycol. The residue was then purified by column chromatography (DCM/methanol 29:1 followed by DCM/EtOAc 4:1 v/v) to give iridium complex **14** as a yellow solid (56 mg, 29%); δ_H (700 MHz; CD_2Cl_2; Me_4Si) 9.03 (1H, ddd, *J* 5.7, 1.7, 0.8, H_{A6}), 8.49 (1H, d, *J* 8.5, H_{A3}), 8.27 (1H, d, *J* 8.5, H_{C3}), 8.10 (1H, ddd, *J* 5.7, 1.7, 0.8, H_{C6}), 8.00 (1H, td, *J* 8.0, 7.4, 1.6, H_{A4}), 7.85 (1H, ddd, *J* 8.2, 7.4, 1.7, H_{E4}), 7.82 (1H, ddd, *J* 8.4, 7.6, 1.6, H_{C4}), 7.73 (1H, dd, *J* 8.0, 1.1, H_{E3}), 7.52 (1H, dd, *J* 8.8, 6.0, H_{F3}), 7.47 (1H, ddd, *J* 5.7, 1.7, 0.8, H_{E6}), 7.35 (1H, ddd, *J* 7.3, 5.7, 1.4, H_{A5}), 6.98 (1H, ddd, *J* 7.4, 5.8, 1.4, H_{C5}), 6.96 (1H, ddd, *J* 7.4, 5.8, 1.4, H_{E5}), 6.33 (1H, dd, *J* 10.6, 8.8, H_{F4}), 5.93 (1H, d, *J* 10.5, H_{B6}), 5.71 (1H, d, *J* 10.5, H_{D6}), 3.20 (3H, s, $H_{B/D7}$), 3.19 (3H, s, $H_{B/D7}$), 2.74 (3H, s, H_{F7}); δ_F (376 MHz, $CDCl_3$, Me_4Si) −105.39 (1F, dd, *J* 10.1, 6.2), −105.70 (1F, dd, *J* 10.1, 2.8), −106.70 (1F, dd, *J* 9.9, 2.6), −109.10 (1F, s), −109.94 (1F, s); δ_C (176 MHz, $CDCl_3$, Me_4Si) 167.68 (C_{F1}), 163.85 (C_{C2}), 162.72 (C_{A2}), 162.45 (C_{F5}), 159.03 (C_{B5}, *J* 262.5), 158.33 (C_{D5}, *J* 272.9), 155.38 (C_{E2}), 150.91 (C_{C6}), 150.41 (C_{E6}), 149.08 (C_{A6}), 139.94 (C_{A4}), 139.68 (C_{C4}), 139. 53 (C_{E4}), 136.07 (C_{F3}), 131.78 (C_{D1}), 130.56 (C_{B1}), 125.92 (C_{E3}), 125.71 (C_{F2}), 124.98 (C_{A3}), 124.51 (C_{C3}), 124.26 (C_{A5}), 123.82 (C_{E5}), 123.19 (C_{C5}), 120.95 (C_{F6}), 117.23 (C_{B6}, d, *J* 18.1), 116.46 (C_{D6}, d, *J* 17.8), 104.60 (C_{F4}, d, *J* 24.1), 46.33 (C_{B+D7}), 45.49 (C_{F7}); HRMS (FTMS+ESI): calcd for $[C_{36}H_{25}F_5N_3O_7S_3{}^{191}Ir+H]^+$: 994.0459. Found: 994.0478.

Iridium Complex ***15***. $IrCl_3{\cdot}3H_2O$ (136 mg, 0.39 mmol) was added to a stirred solution of 2-(2,4-difluoro-3-[(4-methylbenzene)sulfonyl]-phenyl)pyridine **7** (293 mg, 0.85 mmol) in 2-ethoxyethanol (10 mL). The mixture was heated to reflux at 130 °C under argon overnight. The mixture was then left to cool, and the solvent was removed in vacuo to leave a yellow solid, presumed to be the bis(μ-Cl) dimer, which was used without further purification. The dimer was dissolved in ethylene glycol (8 mL), and the 2-(2,4-difluoro-3-[(4-

DOI: 10.1021/acs.inorgchem.6b01179
Inorg. Chem. 2016, 55, 8612−8627

methylbenzene)sulfonyl]phenyl)pyridine **7** (130 mg, 0.38 mmol), NEt_3 (0.1 mL), and acetylacetone (0.1 mL) were added. The reaction procedure and workup as described for **14** gave iridium complex **15** as a yellow solid (110 mg, 23%); Anal. Calcd for $C_{54}H_{37}N_3F_5O_7S_3Ir$: C, 53.11; H, 2.89; N, 3.44. Found: C, 52.64; H, 2.89; N, 3.37%; δ_H (400 MHz; $CDCl_3$; Me_4Si) 8.36 (1H, d, *J* 8.5), 8.25 (1H, d, *J* 8.5), 7.93 (3H, dd, *J* 6.3, 1.8), 7.89−7.78 (4H, m), 7.71 (2H, tdd, *J* 8.1, 6.2, 1.7), 7.62−7.55 (1H, m), 7.42 (1H, dd, *J* 8.9, 6.0), 7.36−7.26 (3H, m), 7.15−7.05 (2H, m), 6.99−6.91 (2H, m), 6.91−6.76 (5H, m), 6.28 (1H, dd, *J* 10.4, 8.8), 5.92 (1H, d, *J* 10.3), 5.40 (1H, d, *J* 10.6), 2.41 (3H, s), 2.37 (3H, s), 2.19 (3H, s); δ_F (376 MHz; $CDCl_3$; Me_4Si) −105.11, −105.21 (2F, m), −108.21 (1F, dd, *J* 10.7, 3.1), −108.35 (1F, d, *J* 4.3), −108.90, −108.97 (1F, m); HRMS (FTMS+ESI): calcd for $[C_{54}H_{37}F_5N_3O_7S_3{}^{191}Ir+H]^+$: 1222.13925. Found: 1222.13928. Crystals for X-ray analysis were grown by slow evaporation of a solution of **15** in DCM/hexane/MeOH (1:2:1 v/v) at RT.

*2-(2-Fluoro-4-methoxyphenyl)-pyridine) (**16**).* A solution of 2-fluoro-4-methoxyphenylboronic acid (1.00 g, 5.88 mmol) and 2-bromopyridine (0.62 mL, 6.46 mmol) in dioxane (30 mL) was degassed by bubbling argon for 30 min. An aqueous solution of Na_2CO_3 (0.79 g, 7.44 mmol in 4 mL) was added, followed by $Pd(PPh_3)_4$ (70 mg, 0.06 mmol). The mixture was heated to 95 °C overnight under argon, then allowed to cool, and the solvent was removed in vacuo. Water and DCM were added, and the organic layer was separated. The aqueous layer was extracted with more DCM, dried over $MgSO_4$, and the solvent was removed in vacuo. The crude oil was purified by distillation using a Kuglerohr apparatus. Residual 2-bromopyridine distilled first (70−80 °C, 0.75 mbar), followed at 115 °C, 0.75 mbar by 2-(2-fluoro-4-methoxyphenyl)-pyridine) **16** as a pale yellow oil (1.09 g, 91%); δ_H (400 MHz; $CDCl_3$; Me_4Si) 8.68 (1H, ddd, *J* 4.8, 1.8, 1.0), 7.95 (1H, t, *J* 9.0), 7.67−7.77 (2H, m), 7.18 (1H, ddd, *J* 7.0, 4.9, 1.5), 6.81 (1H, ddd, *J* 8.8, 2.5, 0.7), 6.69 (1H, dd, *J* 13.2, 2.5), 3.83 (3H,s); δ_F (376 MHz, $CDCl_3$, Me_4Si) −114.74 (1F, t, *J* 12.3); δ_C (101 MHz; $CDCl_3$; Me_4Si) 161.47 (d, J_{C-F} 11.2), 161.32 (d, J_{C-F} 249.5), 153.43 (d, J_{C-F} 2.8), 149.68 (s), 136.40 (s), 131.63 (d, J_{C-F} 4.9), 124.03 (d, J_{C-F} 9.8), 121.85 (s), 120.01 (d, J_{C-F} 11.9), 110.65 (d, J_{C-F} 2.9), 102.00 (d, J_{C-F} 27.0), 55.72 (s); HRMS (FTMS +ESI): calcd for $[C_{12}H_{10}NFO+H]^+$: 204.0825. Found: 204.0817.

*2-(2-Fluoro-4-methoxyphenyl)-4-mesitylpyridine (**17**).* A solution of 2-chloro-4-(2,4,6-trimethylphenyl)pyridine[33a] (1.23 g, 5.31 mmol), 2-fluoro-4-methoxyphenylboronic acid (1.00 g, 5.88 mmol), palladium(II) acetate (73 mg, 0.36 mmol), and triphenylphosphine (363 mg, 1.52 mmol) in 1,2-dimethoxyethane (DME; 60 mL) was degassed with argon for 30 min. A 2 M aqueous solution of sodium carbonate (11 mL, 2.31 g, 24.01 mmol) was degassed for 25 min. The solutions were combined, and the mixture was heated to reflux (105 °C) under argon for 24 h. The reaction mixture was then cooled to RT, and the DME was removed in vacuo. DCM (50 mL) was then added, followed by brine (50 mL). The organic layer was separated and dried over $MgSO_4$. The solvent was removed in vacuo, and the residue was purified by column chromatography (EtOAc/hexane 1:5 v/v) to give 2-(2-fluoro-4-methoxyphenyl)-4-mesitylpyridine **17** as a yellow oil (1.35 g, 78%); δ_H (400 MHz; $CDCl_3$; Me_4Si) 8.73 (1H, dd, *J* 4.9, 0.9), 8.02 (1H, t, *J* 9.0), 7.55−7.61 (1H, m), 7.03 (1H, dd, *J* 5.0, 1.5), 6.94−6.99 (2H, m), 6.84 (1H, ddd, *J* 8.8, 2.5, 0.7), 6.69 (1H, dd, *J* 13.1, 2.5), 3.85 (3H, s), 2.34 (3H, s), 2.05 (6H, s); δ_F (376 MHz, $CDCl_3$, Me_4Si) −114.38 (1F, t, *J* 13.2); δ_C (101 MHz; $CDCl_3$; Me_4Si) 161.28 (d, *J* 250.1), 161.41 (d, *J* 11.4), 153.50 (d, *J* 2.8), 149.79 (s), 149.69 (s), 137.48 (s), 136.51 (s), 135.28 (s), 131.59 (d, *J* 4.8), 128.33 (s), 125.00 (d, *J* 9.8), 122.86 (s), 119.95 (d, *J* 11.6), 110.58 (d, *J* 3.0), 101.93 (d, *J* 27.2), 55.67 (s), 21.05 (s), 20.62 (s); HRMS (FTMS +ESI): calcd for $[C_{21}H_{20}FNO+H]^+$: 322.1607. Found: 322.1608.

*2-(2-Fluoro-3-iodo-4-(methoxyphenyl)-pyridine) (**18**).* The reaction used the general procedure for lithiation followed by iodination using ^{n}BuLi (1.94 mL, 2.5 M), DIPA (0.75 mL, 5.34 mmol), 2-(2-fluoro-4-methoxyphenyl)-pyridine) **16** (790 mg, 3.89 mmol), I_2 (1.38 g, 5.44 mmol), and THF (35 mL). Purification by column chromatography (hexane/EtOAc 3:2 v/v) gave 2-(2-fluoro-3-iodo-4-methoxyphenyl)-pyridine) **18** (746 mg, 58%) as an off-white solid; mp 107.2−109.7 °C; δ_H (400 MHz; $CDCl_3$ Me_4Si) 8.69 (1H, dt, *J* 4.8, 1.5), 7.98 (1H, t, *J* 8.8), 7.71−7.78 (2H, m), 7.19−7.28 (1H, m), 6.76 (1H, dd, *J* 8.8, 1.2), 3.96 (3H, s); δ_F (376 MHz; $CDCl_3$; Me_4Si) −93.14 (d, *J* 10.7); δ_C (101 MHz; $CDCl_3$ Me_4Si) 160.09 (d, *J* 248.0), 160.33 (d, *J* 6.1), 152.82 (d, *J* 3.3), 149.79, 136.62, 131.84 (d, *J* 4.8), 124.23 (d, *J* 9.6), 122.33, 121.25 (d, *J* 14.9), 106.97 (d, *J* 2.9), 75.06 (d, *J* 28.96), 57.02; HRMS (FTMS+ESI): calcd for $[C_{12}H_9NFOI+H]^+$: 329.9791. Found: 329.9787.

*2-(2-Fluoro-3-iodo-4-methoxyphenyl)-4-(2,4,6-trimethylphenyl)-pyridine (**19**).* The general procedure for lithiation followed by iodination used ^{n}BuLi (2.1 mL, 2.5 M), DIPA (0.81 mL, 5.78 mmol), 2-(2-fluoro-4-methoxyphenyl)-4-mesitylpyridine **17** (1.35 g, 4.20 mmol), I_2 (1.49 g, 8.09 mmol), and THF (30 mL, dry). The reaction was worked up as described in the general method, and the product was then purified by column chromatography (hexane/EtOAc 2:1) to give an off-white solid, 2-(2-fluoro-3-iodo-4-methoxyphenyl)-4-mesitylpyridine) **19** (1.03 g, 55%); mp 167.4−168.5 °C; δ_H (400 MHz; $CDCl_3$; Me_4Si) 8.73 (1H, dd, *J* 5.0, 0.9), 8.05 (1H, t, *J* 8.8), 7.54−7.61 (1H, m), 7.06 (1H, dd, *J* 5.0, 1.5), 6.96 (2H, s), 6.78 (1H, dd, *J* 8.8, 1.1), 3.97 (3H, s), 2.34 (3H, s), 2.05 (6H, s); δ_F (376 MHz, $CDCl_3$, Me_4Si) −92.81 (d, *J* 12.6); δ_C (101 MHz; $CDCl_3$; Me_4Si) 159.98 (d, *J* 248.3), 160.21 (d, *J* 6.1), 152.81 (d, *J* 3.3), 150.05, 149.76, 137.55, 136.27, 135.17, 131.73 (d, *J* 4.9), 128.34, 125.21 (d, *J* 9.7), 123.27, 121.17 (d, *J* 14.5), 106.83 (d, *J* 2.9), 74.96, 56.88, 21.05, 20.62; HRMS (FTMS+ESI): calcd for $[C_{21}H_{19}NFOI+H]+$: 448.0574. Found: 448.0565.

*2-(2-Fluoro-4-methoxy-3-(methylsulfonyl)phenyl)pyridine (**20**).* The reaction followed the general procedure for sulfone synthesis using 2-(2-fluoro-3-iodo-4-methoxyphenyl)-pyridine) **18** (1.02 g, 3.11 mmol), CuI (0.89 g, 4.67 mmol), and $MeSO_2Na$ (0.51 g, 4.98 mmol) in DMF (2.5 mL). The product was purified by column chromatography (DCM/EtOAc 1:1 v/v) to give 2-(2-fluoro-4-methoxy-3-(methylsulfonyl)phenyl)pyridine **20** (390 mg, 45%); δ_H (400 MHz; $CDCl_3$; Me_4Si) 8.70 (1H, dt, *J* 4.8, 1.4), 8.23 (1H, dd, *J* 9.0, 8.3), 7.72−7.82 (2H, m), 7.26−7.30 (1H, m), 6.98 (1H, dd, *J* 8.9, 1.3), 4.03 (3H, s), 3.34 (3H, s); δ_F (376 MHz; $CDCl_3$; Me_4Si) −113.56 (d, *J* 9.3); δ_C (176 MHz; $CDCl_3$; Me_4Si) 159.07 (d, *J* 3.4), 158.4 (d, *J* 263.2), 151.87 (d, *J* 1.7), 149.96, 136.87 (d, *J* 6.1), 136.72, 124.60 (d, *J* 9.8), 122.80, 122.20 (d, *J* 14.3), 118.01 (d, *J* 13.6), 108.66 (d, *J* 3.5), 57.28, 45.61; HRMS (FTMS+ESI): calcd for $[C_{13}H_{12}NFO_3S+H]^+$: 282.0600. Found: 282.0615.

*2-(2-Fluoro-4-methoxy-3-[methylsulfonyl]phenyl)-4-(2,4,6-trimethylphenyl)pyridine (**21**).* The reaction followed the general procedure for sulfone synthesis using 2-(2-fluoro-3-iodo-4-methoxyphenyl)-4-mestitylpyridine) **19** (1.00 g, 2.24 mmol), CuI (0.68 g, 3.58 mmol), $MeSO_2Na$ (0.34 g, 3.35 mmol), and DMF (3.5 mL, dry). The reaction was worked up as described in the general procedure, and the product was purified by column chromatography (DCM/EtOAc 1:1) to give 2-(2-fluoro-4-methoxy-3-(methylsulfonyl)phenyl)-4-mesitylpyridine **21** (470 mg, 53%); mp 169.2−170.8 °C; (400 MHz; $CDCl_3$; Me_4Si) 8.74 (1H, d, *J* 5.0), 8.30 (1H, t, *J* 8.6), 7.57−7.63 (1H, m), 7.10 (1H, dd, *J* 5.0, 1.5), 7.00 (1H, dd, *J* 9.0, 1.2), 6.92−6.97 (2H, m), 4.05 (3H, s), 3.32 (3H, s), 2.33 (3H, s), 2.03 (6H, s); δ_F (376 MHz; $CDCl_3$; Me_4Si) −113.44 (d, *J* 9.5); δ_C (176 MHz; $CDCl_3$; Me_4Si) 159.09 (d, *J* 3.3), 158.49 (d, *J* 263.0), 152.00, 150.46, 150.07, 137.77, 136.91 (d, *J* 5.9), 136.11, 135.17, 128.49, 125.72 (d, *J* 8.9), 123.89, 122.24 (d, *J* 14.0), 118.06 (d, *J* 13.3), 108.68 (d, *J* 3.4), 57.29, 45.61, 21.18, 20.74; HRMS (FTMS+ESI): calcd for $[C_{22}H_{22}NFO_3S+H]^+$: 400.1383. Found: 400.1379.

*2-(2-Fluoro-4-methoxy-3-(p-toluenesulfonyl)phenyl)-4-mesitylpyridine (**22**).* The reaction followed the general procedure for sulfone synthesis using 2-(2-fluoro-3-iodo-4-methoxyphenyl)-4-mesitylpyridine **19** (0.81 g, 1.81 mmol), sodium *p*-tolylsulfinate (0.52 g, 2.90 mmol), CuI (0.52 g, 2.71 mmol), and DMF (3 mL). The product was purified by column chromatography (5% EtOAc in DCM, increased to 20%) to give 2-(2-fluoro-4-methoxy-3-(*p*-toluenesulfonyl)phenyl)-4-mesitylpyridine **22** as an off white solid (0.17 g, 21%); δ_H (400 MHz; $CDCl_3$; Me_4Si) 8.73 (1H, dd, *J* 5.0, 0.9), 8.22 (1H, dd, *J* 8.9, 8.2), 7.88−7.98 (2H, m), 7.56−7.66 (1H, m), 7.26−7.33 (2H, m), 7.08 (1H, dd, *J* 5.0, 1.5), 6.94−6.99 (2H, m), 6.87 (1H, dd, *J* 9.0, 1.2), 3.85 (3H, s), 2.41 (3H, s), 2.34 (3H, s) 2.04 (6H, s); δ_F (376 MHz; $CDCl_3$;

DOI: 10.1021/acs.inorgchem.6b01179
Inorg. Chem. 2016, 55, 8612−8627

Me_4Si) −112.69 (1F, d, *J* 10.9); δ_C (101 MHz; $CDCl_3$; Me_4Si) 158.40 (d, *J* 263.0), 158.98 (d, *J* 3.3), 152.10 (d, *J* 1.8), 150.26, 149.88, 144.17, 139.92, 137.63, 136.68 (d, *J* 6.1), 136.05, 135.10, 129.26, 128.36, 127.82, 125.62 (d, *J* 9.9), 123.64, 121.78 (d, *J* 14.2), 118.64 (d, *J* 13.4), 108.61 (d, *J* 3.6), 56.77, 21.65, 21.07, 20.64; HRMS (FTMS+ESI): calcd for $[C_{28}H_{26}NFO_3S+H]^+$: 476.1696. Found: 476.1718.

Iridium Complex ***23***. The reaction followed the general procedure for the synthesis of iridium pic complexes, Method B, using $IrCl_3 \cdot 3H_2O$ (233 mg, 0.66 mmol), 2-(2-fluoro-4-methoxy-3-(methylsulfonyl)phenyl)pyridine **20** (390 mg, 1.39 mmol), picolinic acid (284 mg, 2.31 mmol), and 2-ethoxyethanol (12 mL). Purification by column chromatography (5% MeOH in DCM) gave a yellow solid, which was suspended in ethanol and heated to reflux. The solution was filtered to afford complex **23** as a yellow solid (310 mg, 54%); Anal. Calcd for $C_{32}H_{26}N_3F_2O_8S_2Ir$: C, 43.93; H, 3.00; N, 4.80. Found: C, 44.02; H, 3.26; N, 4.97%; δ_H (700 MHz; $CDCl_3$; Me_4Si) 8.78 (1H, ddd, *J* 5.8, 1.7, 0.8, H_{A6}), 8.37 (1H, ddd, *J* 7.8, 1.5, 0.8, H_{E3}), 8.34 (1H, d, *J* 8.5, H_{B3}), 8.27 (1H, d, *J* 8.5, H_{A3}), 8.02 (1H, td, *J* 7.8, 1.6, H_{E4}), 7.84 (1H, td, H_{B4}) 7.82 (1H, td, J, H_{A4}), 7.79 (1H, ddd, *J*, H_{E6}), 7.52 (1H, ddd, *J* 7.7, 5.4, 1.5, H_{E5}), 7.46 (1H, ddd, *J* 5.9, 1.6, 0.8, H_{B6}), 7.23 (1H, ddd, *J* 7.3, 5.8, 1.4, H_{A5}), 7.03 (1H, ddd, *J* 7.4, 5.8, 1.4, H_{B5}), 5.73 (1H, s, H_{C6}), 5.57 (1H, s, H_{D6}), 3.56 (3H, s, H_{C8}), 3.51 (3H, s, H_{D8}), 3.25 (3H, s, H_{C7}), 3.20 (3H, s, H_{D7}); δ_F (376 MHz; $CDCl_3$; Me_4Si) −112.10 (1F, s), −112.58 (1F, s); δ_C (176 MHz; $CDCl_3$; Me_4Si) 172.31 (s, C_{E7}), 165.37 (d, *J* 6.2, C_{B2}), 164.21 (d, *J* 6.2, C_{A2}), 161.38 ($C_{C/D2}$), 160.56 ($C_{C/D2}$), 158.69 (d, *J* 3.0, C_{C5}), 158.40 (d, *J* 284.0, C_{C3}), 158.30 (d, *J* 284.0, C_{D3}), 158.18 (d, *J* 2.6, C_{D5}), 151.18 (s, C_{E2}), 148.64 (s, C_{A6}), 148.26 (s, C_{E6}), 148.00 (s, C_{B6}), 138.90(s, C_{E4}), 138.73 (s, $C_{A/B4}$), 138.70 (s, $C_{A/B4}$), 128.81 (s, C_{E3}), 128.78 (s, C_{E5}), 126.12 (d, J,C_{C1}), 125.81 (d, C_{D1}), 123.53 (d, J, C_{B3}), 122.96 (d, J, C_{A3}), 122.41 (s, C_{B5}), 122.35 (s, C_{A5}), 111.28 (d, *J* 11.4, C_{D4}), 111.01 (C_{D6}), 110.93 (d, *J* 11.5, C_{C4}), 110.73 (C_{C6}), 56.09 (s, C_{C8}), 55.97 (s, C_{D8}), 45.29 (s, $C_{C/D7}$), 45.28 (s, $C_{C/D7}$); HRMS (FTMS+ESI): calcd for $[C_{32}H_{26}N_3F_2O_8S_2{}^{191}Ir+H]^+$: 874.0814. Found: 874.0786. Crystals for X-ray analysis were grown by slow vapor diffusion of pentane into a solution of **23** in DCM.

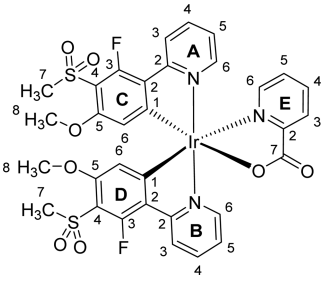

Iridium Complex ***24***. The reaction followed the general procedure for the synthesis of iridium pic complexes, Method B, using $IrCl_3 \cdot 3H_2O$ (189 mg, 0.54 mmol), 2-(2-fluoro-4-methoxy-3-(methylsulfonyl)phenyl)-4-mesitylpyridine **21** (450 mg, 1.13 mmol), picolinic acid (231 mg, 1.88 mmol), and 2-ethoxyethanol (20 mL). The reaction was worked up as described in the general procedure, and the residue was purified by column chromatography (5% MeOH in DCM). The yellow solid was suspended in ethanol and heated to reflux. The solution was filtered hot to afford Ir complex **24** as a yellow solid (420 mg, 70%). Anal. Calcd for $C_{50}H_{46}N_3F_2O_8S_2Ir \cdot CH_2Cl_2$: C, 51.21; H, 4.04; N, 3.51. Found: C, 51.34; H, 3.99; N, 3.55%; δ_H (400 MHz; $CDCl_3$; Me_4Si) 8.80−8.87 (m, 1H), 8.44 (1H, dt, *J* 7.8, 0.9), 8.19 (1H, s), 8.12 (1H, s), 8.07 (1H, td, *J* 7.7, 1.5), 7.88 (1H, dt, *J* 5.1, 1.3), 7.57 (1H, ddd, *J* 7.6, 5.3, 1.5), 7.45 (1H, d, *J* 5.9), 7.09 (1H, dd, *J* 5.9, 1.8), 6.93−7.02 (4H, m), 6.87 (1H, dd, *J* 5.9, 1.8), 5.83 (1H, s), 5.77 (1H, s), 3.61 (3H, s), 3.58 (3H, s), 3.23 (3H, s), 3.19 (3H, s), 2.34 (6H, s), 2.09 (3H, s), 2.05 (3H, s), 2.00 (3H, s), 1.95 (3H, s); δ_F (376 MHz; $CDCl_3$; Me_4Si) −111.68 (s), −112.28 (s); HRMS (FTMS +ESI): calcd for $[C_{50}H_{46}N_3F_2O_8S_2{}^{191}Ir+H]^+$: 1110.2379. Found: 1110.2393.

Iridium Complex ***25***. The reaction followed the general procedure for the synthesis of iridium pic complexes, Method B, using $IrCl_3 \cdot 3H_2O$ (72 mg, 0.20 mmol), 2-(2-fluoro-4-methoxy-3-(*p*-toluenesulfonyl)phenyl)-4-mesitylpyridine **22** (184 mg, 0.42 mmol), picolinic acid (37 mg, 0.30 mmol), and 2-ethoxyethanol (5 mL). The product was purified initially by column chromatography (EtOAc in DCM 1:4, increased to 1:3 v/v) to give a yellow solid, which was further purified by recrystallization from ethanol to give complex **25** (210 mg, 83%); Anal. Calcd for $C_{62}H_{54}N_3F_2O_8S_2Ir$: C, 58.94; H, 4.31; N, 3.33. Found: C, 58.60; H, 4.26; N, 3.27%; δ_H (400 MHz; $CDCl_3$; Me_4Si) 8.74 (1H, d, *J* 5.8), 8.39 (1H, d, *J* 7.8), 8.15 (1H, s), 8.08 (1H, s), 8.04 (1H, td, *J* 7.7, 1.6), 7.85−7.90 (2H, m) 7.77−7.85 (3H, m), 7.56 (1H, ddd, *J* 7.4, 5.3, 1.1), 7.40 (1H, d, *J* 5.9), 7.30−7.20 (4H, m), 7.03−6.92 (5H, m), 6.81 (1H, dd, *J* 5.9, 1.8), 5.71 (1H, s), 5.63 (1H, s), 3.43 (3H, s), 3.37 (3H, s), 2.38 (6H, s), 2.34 (6H, s), 2.08 (3H, s), 2.00 (3H, s), 1.96 (3H, s), 1.94 (3H, s); δ_F (376 MHz; $CDCl_3$; Me_4Si) −110.60 (1F, s), −111.33 (1F, s); HRMS (FTMS+ESI): calcd for $[C_{62}H_{54}N_3F_2O_8S_2{}^{191}Ir+H]^+$: 1262.3005. Found: 1262.3020.

(2,4-Dimethoxy-3-(methylthio)phenyl)boronic Acid ***27***. ^{n}BuLi (11.25 mL, 2.5 M in hexanes) was added dropwise to a stirred solution of 3-bromo-2,6-dimethoxythioanisole **26**[42] (6.17 g, 23.45 mmol) in THF (15 mL, dry) at −78 °C. The mixture was stirred at −78 °C for 1 h. Triisopropylborate (8.11 mL, 35.15 mmol) was slowly added, and the reaction mixture was stirred at −78 °C for 1 h before being left to warm to RT overnight. Dilute HCl was added, and the solution was extracted with EtOAc. The solvent was removed in vacuo to leave a sticky brown solid, which was redissolved in EtOAc and was extracted with aqueous KOH (150 mL). The aqueous layer was acidified to pH 5 with dilute HCl and extracted with EtOAc. The solvent was removed in vacuo to give a beige solid, (2,4-dimethoxy-3-(methylthio)phenyl)boronic acid **27** (2.80 g, 52%); δ_H (400 MHz; $CDCl_3$; Me_4Si) 7.80 (1H, d, *J* 8.4), 6.79 (1H, d, *J* 8.4), 5.88 (2H, br s), 3.98 (3H, s), 3.97 (3H, s), 2.42 (3H, s); δ_B (128 MHz; $CDCl_3$; Me_4Si) 28.66 (1B, br s); HRMS (FTMS+ESI): calcd for $[C_9H_{13}O_4S^{10}B+H]^+$: 228.0742. Found: 228.0732.

2-(2,4-Dimethoxy-3-(methylthio)phenyl)-4-mesitylpyridine ***28***. 2-Chloro-4-mesitylpyridine (0.72 g, 3.11 mmol), (2,4-dimethoxy-3-(methylthio)phenyl)boronic acid **27** (0.85 g, 3.73 mmol), and PPh_3 (211 mg, 0.80 mmol) were dissolved in DME (50 mL), and the solution was degassed for 20 min by bubbling with argon. An aqueous solution of Na_2CO_3 (1.34 g, 12.64 mmol in 10 mL) was degassed for 20 min. The solutions were combined, and $Pd(OAc)_2$ (43 mg, 0.19 mmol) was added. The mixture was heated to reflux for 24 h before being cooled. The solvent was removed under reduced pressure, and DCM and water were added. The organic layer was separated, and the aqueous layer was extracted with further DCM. The extracts were combined, and the solvent was removed. The residue was purified by column chromatography (DCM/EtOAc 1:1 v/v) to give a white solid, 2-(2,4-dimethoxy-3-(methylthio)phenyl)-4-mesitylpyridine **28** (0.70 g, 60%); mp 133.4−136.2; δ_H (400 MHz; CD_3OD; Me_4Si) 8.65 (1H, dd, *J* 5.1, 0.9), 7.62 (1H, d, *J* 8.6), 7.58−7.52 (1H, m), 7.16 (1H, dd, *J* 5.1, 1.6), 6.97 (2H, s), 6.97 (1H, d, *J* 8.7), 3.94 (3 H, s), 3.57 (3 H, s), 2.39 (3H, s), 2.31 (3H, s), 2.05 (6H, s); δ_C ^{13}C NMR (101 MHz, CD_3OD; Me_4Si) 161.38, 159.22, 156.10, 150.69, 148.72, 137.40, 136.03, 134.50, 130.81, 127.99, 126.57, 126.07, 123.18, 119.02, 107.31, 99.99, 19.73, 19.34, 16.60; HRMS (FTMS+ESI): calcd for $[C_{23}H_{25}NFO_2S+H]^+$: 380.1684. Found: 380.1666.

2-(2,4-Dimethoxy-3-(methylthio)phenyl)-4-mesitylpyridinium Chloride ***29***. HCl (0.05 mL, 12 M) was added to a stirred solution of 2-(2,4-dimethoxy-3-(methylthio)phenyl)-4-mesitylpyridine **28** (236 mg, 0.62 mmol) in DCM/MeOH (40 mL, 1:1), and the mixture was stirred at RT overnight. The solvent was removed in vacuo to leave the product as a white solid, 2-(2,4-dimethoxy-3-(methylthio)-phenyl)-4-mesitylpyridinium chloride **29** (259 mg, 100%); mp 177.3−180.2 °C; δ_H (400 MHz; CD_3OD; Me_4Si) 8.84 (1H, d, *J* 6.1), 8.18−8.12 (m, 1H), 7.87 (1H, dd, *J* 6.1, 1.9), 7.74 (1H, dd, *J* 8.8, 0.9), 7.12 (1H, d, *J* 8.8), 7.09−7.08 (2H, m), 4.03 (s, 3H), 3.75 (s, 3H), 2.47 (s, 3H), 2.37 (s, 3H), 2.14 (s, 6H); δ_C (176 MHz, CD_3OD; Me_4Si) 164.17, 160.76, 159.45, 150.20, 140.89, 139.28, 134.22, 133.75, 130.94, 128.91, 128.51, 126.27, 120.38, 117.78, 109.99, 108.05, 99.79, 60.89, 55.66, 22.77, 19.71, 19.16, 16.28.

DOI: 10.1021/acs.inorgchem.6b01179
Inorg. Chem. 2016, 55, 8612−8627

2-(2,4-Dimethoxy-3-(methylsulfonyl)phenyl)-4-mesitylpyridine ***30***. *m*-Chloroperoxybenzoic acid (436 mg, 2.68 mmol) was added to a stirred solution of 2-(2,4-dimethoxy-3-(methylthio)phenyl)-4-mesitylpyridinium chloride **29** (510 mg, 1.22 mmol) in DCM (20 mL). The solution was stirred at RT overnight. The reaction was quenched with aqueous $NaHSO_3$, and the organic layer was separated. The aqueous layer was extracted with additional DCM. The organic layers were then washed with aqueous NaOH before the solvent was removed in vacuo, and the residue was purified by reverse-phase column chromatography (water/MeOH) to give a white solid, 2-(2,4-dimethoxy-3-(methylsulfonyl)phenyl)-4-mesitylpyridine **30** (420 mg, 83%); mp 155.8−160.8 °C, which started to discolour at 148.7 °C; δ_H (400 MHz; $CDCl_3$; Me_4Si) 8.75 (1H, dd, *J* 5.0, 0.9), 8.05 (1H, d, *J* 8.9), 7.70 (1H, dd, *J* 1.6, 0.9), 7.09 (1H, dd, *J* 5.0, 1.6), 6.98 (1H, d, *J* 8.9), 6.96 (2 H, s), 4.00 (3 H, s), 3.61 (3 H, s), 3.33 (3 H, s), 2.33 (3 H, s), 2.03 (6 H, s); δ_C (101 MHz, $CDCl_3$, Me_4Si) 158.95, 158.44, 154.71, 150.38, 149.99, 137.74, 137.21, 136.22, 135.07, 128.45, 128.14, 125.69, 123.55, 123.44, 109.10, 63.42, 56.97, 46.25, 21.16, 20.74; HRMS (FTMS+ESI): calcd for $[C_{23}H_{25}NFO_4S+H]^+$: 412.1583. Found: 412.1564.

Iridium Complex ***31***. $[Ir(cod)Cl]_2$ (51 mg, 0.19 mmol) was added to a stirred solution of 2-(2,4-dimethoxy-3-(methylsulfonyl)phenyl)-4-mesitylpyridine **30** (130 mg, 0.32 mmol) in 2-ethoxyethanol (5 mL). The solution was heated to 130 °C under argon overnight, picolinic acid (26 mg, 0.21 mmol) was added, and the solution was heated at 130 °C for 6 h under argon. The solution was cooled, and the solvent was removed in vacuo. The residue was purified by column chromatography (DCM/CH_3CN 2:1 v/v) to give a yellow solid, iridium complex **31** (70 mg, 40%); Anal. Calcd for $C_{52}H_{52}N_3O_{10}S_2Ir\cdot 1.5\ CH_2Cl_2$: C, 50.89; H, 4.37; N, 3.33. Found: C, 50.43; H, 3.97; N, 3.08%; δ_H (400 MHz; $CDCl_3$; Me_4Si) 8.84 (1H, d, *J*), 8.50 (1H, dd, *J* 1.8, 0.7 Hz), 8.45 (1H, d, *J* 7.7), 8.37 (1H, dd, *J* 1.8, 0.7), 8.04 (1H, td, *J* 7.8, 1.6), 7.84 (1H, d, *J* 5.3), 7.53 (1H, ddd, *J* 7.4, 5.4, 1.5), 7.45 (1H, d, *J* 5.9), 7.05 (1H, dd, *J* 5.9, 1.9), 7.04−6.96 (4H, m), 6.81 (1H, dd, *J* 5.9, 1.9), 5.83 (1H, s), 5.78 (1H, s), 3.92 (3H, s), 3.89 (3H, s), 3.55 (3H, s), 3.54 (3H, s), 3.25 (3H, s), 3.20 (3H, s), 2.35 (6H, s), 2.11 (3H, s), 2.05 (3H, s), 2.00 (3H, s), 1.96 (3H, s); HRMS (FTMS +ESI): calcd for $[C_{52}H_{52}N_3O_{10}S_2{}^{191}Ir+H]^+$: 1134.2778. Found: 1134.2792. Crystals for X-ray analysis were grown by slow evaporation from a DCM/hexane mixture.

■ ASSOCIATED CONTENT

Supporting Information

The Supporting Information is available free of charge on the ACS Publications website at DOI: 10.1021/acs.inorgchem.6b01179.

Thermal data; photophysical data; cyclic voltammograms; computational data; copies of NMR spectra (PDF)

X-ray crystallographic data including files in CIF format with CCDC Nos. 1413092−1413097 and 1474568 (ZIP)

■ AUTHOR INFORMATION

Corresponding Author

*E-mail: m.r.bryce@durham.ac.uk.

Notes

The authors declare no competing financial interest.

■ ACKNOWLEDGMENTS

We thank Durham Univ. for a doctoral scholarship (to H.B.), EPSRC Grant No. EP/L0261X/1 for funding, and Dr. D. S. Yufit for solving the X-ray crystal structure of complex **23**.

■ REFERENCES

(1) Yam, V. W.-W.; Wong, K. M.-C. *Chem. Commun.* **2011**, *47*, 11579−11592.
(2) Baldo, M. A.; Lamansky, S.; Burrows, P. E.; Thompson, M. E.; Forrest, S. R. *Appl. Phys. Lett.* **1999**, *75*, 4−6.
(3) Lowry, M. S.; Bernhard, S. *Chem. - Eur. J.* **2006**, *12*, 7970−7977.
(4) Lo, K. K.-W.; Hui, W.-K.; Chung, C.-K.; Tsang, K. H.-K.; Ng, D. C.-M.; Zhu, N.; Cheung, K.-K. *Coord. Chem. Rev.* **2005**, *249*, 1434−1450.
(5) Müllen, K.; Scherf, U. *Organic Light-Emitting Devices;* Wiley-VCH: Weinheim, Germany, 2006.
(6) Li, Z.; Meng, H. *Organic Light-Emitting Materials and Devices;* CRC Press: Boca Raton, FL, 2006.
(7) *Highly Efficient OLEDs with Phosphorescent Materials;* Yersin, H., Ed.; Wiley-VCH: Weinheim, Germany, 2008.
(8) Mertens, R. *The OLED Handbook. A Guide to OLED Technology, Industry and Market* [Online], 2014. www.oled-info.com/handbook.
(9) Kamtekar, K. T.; Monkman, A. P.; Bryce, M. R. *Adv. Mater.* **2010**, *22*, 572−582.
(10) Ying, L.; Ho, C.-L.; Wu, H.; Cao, Y.; Wong, W.-Y. *Adv. Mater.* **2014**, *26*, 2459−2473.
(11) Holder, E.; Langeveld, B. M. W.; Schubert, U. S. *Adv. Mater.* **2005**, *17*, 1109−1121.
(12) Chou, P.-T.; Chi, Y. *Chem. - Eur. J.* **2007**, *13*, 380−395.
(13) Wong, W.-Y.; Ho, C.-L. *J. Mater. Chem.* **2009**, *19*, 4457−4482.
(14) You, Y.; Park, S. Y. *Dalton Trans.* **2009**, 1267−1282. (b) Ladouceur, S.; Zysman- Colman, E. *Eur. J. Inorg. Chem.* **2013**, *2013*, 2985−3007.
(15) Ragni, R.; Plummer, E. A.; Brunner, K.; Hofstraat, J. W.; Babudri, F.; Farinola, G. M.; Naso, F.; De Cola, L. *J. Mater. Chem.* **2006**, *16*, 1161−1170.
(16) Baranoff, E.; Curchod, B. F. E.; Monti, F.; Steimer, F.; Accorsi, G.; Tavernelli, I.; Rothlisberger, U.; Scopelliti, R.; Grätzel, M.; Nazeeruddin, M. K. *Inorg. Chem.* **2012**, *51*, 799−811.
(17) Lamansky, S.; Djurovich, P.; Murphy, D.; Abdel-Razzaq, F.; Adachi, C.; Burrows, P. E.; Forrest, S. R.; Thompson, M. E.; et al. *J. Am. Chem. Soc.* **2001**, *123*, 4304−4312.
(18) Rausch, A. F.; Thompson, M. E.; Yersin, H. *Inorg. Chem.* **2009**, *48*, 1928−1937.
(19) Chen, S.; Tan, G.; Wong, W.-Y.; Kwok, H.-S. *Adv. Funct. Mater.* **2011**, *21*, 3785−3793.
(20) Ahmed, E.; Earmme, T.; Jenekhe, S. A. *Adv. Funct. Mater.* **2011**, *21*, 3889−3899.
(21) Ho, C.-L.; Chi, L.-C.; Hung, W.-Y.; Chen, W.-Y.; Lin, Y.-C.; Wu, H.; Mondal, E.; Zhou, G.-J.; Wong, K.-T.; Wong, W.-Y. *J. Mater. Chem.* **2012**, *22*, 215−224.
(22) Baranoff, E.; Curchod, B. F. *Dalton Trans.* **2015**, *44*, 8318−8329.
(23) (a) Sajoto, T.; Djurovich, P. I.; Tamayo, A.; Yousufuddin, M.; Bau, R.; Thompson, M. E.; Holmes, R. J.; Forrest, S. R. *Inorg. Chem.* **2005**, *44*, 7992−8003. (b) Darmawan, N.; Yang, C.-H.; Mauro, M.; Raynal, M.; Heun, S.; Pan, J.; Buchholz, H.; Braunstein, P.; De Cola, L. *Inorg. Chem.* **2013**, *52*, 10756−10765. (c) Li, T.-Y.; Liang, X.; Zhou, L.; Wu, C.; Zhang, S.; Liu, X.; Lu, G.-Z.; Xue, L.-S.; Zheng, Y.-X.; Zuo, J.-L. *Inorg. Chem.* **2015**, *54*, 161−173.
(24) (a) Yang, C.-H.; Mauro, M.; Polo, F.; Watanabe, S.; Muenster, I.; Fröhlich, R.; De Cola, L. *Chem. Mater.* **2012**, *24*, 3684−3695. (b) Lee, S.; Kim, S.-O.; Shin, H.; Yun, H.-J.; Yang, K.; Kwon, S.-K.; Kim, J.-J.; Kim, Y.-H. *J. Am. Chem. Soc.* **2013**, *135*, 14321−14328. (c) Park, H. J.; Kim, J. N.; Yoo, H.-J.; Wee, K.-R.; Kang, S. O.; Cho, D. W.; Yoon, U. C. *J. Org. Chem.* **2013**, *78*, 8054−8064.
(25) Lee, S. J.; Park, K.-M.; Yang, K.; Kang, Y. *Inorg. Chem.* **2009**, *48*, 1030−1037.
(26) Lin, C.-H.; Chang, Y.-Y.; Hung, J.-Y.; Lin, C.-Y.; Chi, Y.; Chung, M.-W.; Lin, C.-L.; Chou, P.-T.; Lee, G.-H.; Chang, C.-H.; Lin, W.-C. *Angew. Chem., Int. Ed.* **2011**, *50*, 3182−3186.
(27) Yang, X.; Xu, X.; Zhou, G. *J. Mater. Chem. C* **2015**, *3*, 913−944.
(28) Li, G.; Fleetham, T.; Turner, E.; Hang, X.-C.; Li, J. *Adv. Opt. Mater.* **2015**, *3*, 390−397.

DOI: 10.1021/acs.inorgchem.6b01179
Inorg. Chem. 2016, 55, 8612−8627

(29) Kozhevnikov, V. N.; Dahms, K.; Bryce, M. R. *J. Org. Chem.* **2011**, *76*, 5143−5148.
(30) (a) Oh, H.; Park, K.-M.; Hwang, H.; Oh, S.; Lee, J. H.; Lu, J.-S.; Wang, S.; Kang, Y. *Organometallics* **2013**, *32*, 6427−6436. (b) Frey, J.; Curchod, B. F.; Scopelliti, R.; Tavernelli, I.; Rothlisberger, U.; Nazeeruddin, M. K.; Baranoff, E. *Dalton Trans.* **2014**, *43*, 5667−5679.
(31) (a) Zhang, W.-H.; Zhang, X.-H.; Tan, A. L.; Yong, M. A.; Young, D. J.; Hor, T. S. A. *Organometallics* **2012**, *31*, 553−559. (b) Lepeltier, M.; Dumur, F.; Marrot, J.; Contal, E.; Bertin, D.; Gigmes, D.; Mayer, C. R. *Dalton Trans.* **2013**, *42*, 4479−4486. (c) Li, L.; Wu, F.; Zhang, S.; Wang, D.; Ding, Y.; Zhu, Z. *Dalton Trans.* **2013**, *42*, 4539−4543. (d) Zheng, Y.; Batsanov, A. S.; Edkins, R. M.; Beeby, A.; Bryce, M. R. *Inorg. Chem.* **2012**, *51*, 290−297.
(32) (a) Tordera, D.; Serrano-Perez, J. J.; Pertegas, A.; Orti, E.; Bolink, H. J.; Baranoff, E.; Nazeeruddin, M. K.; Frey, J. *Chem. Mater.* **2013**, *25*, 3391−3397. (b) Seifert, R.; Rabelo de Moraes, I.; Scholz, S.; Gather, M. C.; Lussem, B.; Leo, K. *Org. Electron.* **2013**, *14*, 115−123. (c) Sivasubramaniam, V.; Brodkorb, F.; Hanning, S.; Loebl, H. P.; Elsbergen, V.; Boerner, H.; Scherf, U.; Kreyenschmidt, M. *Cent. Eur. J. Chem.* **2009**, *7*, 836−845. (d) Sivasubramaniam, V.; Brodkorb, F.; Hanning, S.; Loebl, H. P.; van Elsbergen, V.; Boerner, H.; Scherf, U.; Kreyenschmidt, M. *J. Fluorine Chem.* **2009**, *130*, 640−649.
(33) (a) Kozhevnikov, V. N.; Zheng, Y.; Clough, M.; Al-Attar, H. A.; Griffiths, G. C.; Abdullah, K.; Raisys, S.; Jankus, V.; Bryce, M. R.; Monkman, A. P. *Chem. Mater.* **2013**, *25*, 2352−2358. (b) Henwood, A. F.; Bansal, A. K.; Cordes, D. B.; Slawin, A.M. Z.; Samuel, I. D. W.; Zysman-Colman, E. *J. Mater. Chem. C* **2016**, *4*, 3726−3737.
(34) Sun, D.; Zhou, X.; Li, H.; Sun, X.; Zheng, Y.; Ren, Z.; Ma, D.; Bryce, M. R.; Yan, S. *J. Mater. Chem. C* **2014**, *2*, 8277−8284.
(35) (a) Tavasli, M.; Bettington, S.; Perepichka, I. F.; Batsanov, A. S.; Bryce, M. R.; Rothe, C.; Monkman, A. P. *Eur. J. Inorg. Chem.* **2007**, *2007*, 4808−4814. (b) Zhou, G.; Ho, C.-L.; Wong, W.-Y.; Wang, Q.; Ma, D.; Wang, L.; Lin, Z.; Marder, T. B.; Beeby, A. *Adv. Funct. Mater.* **2008**, *18*, 499−511. (c) Ragni, R.; Orselli, E.; Kottas, G. S.; Omar, O. H.; Babudri, F.; Pedone, A.; Naso, F.; Farinola, G. M.; De Cola, L. *Chem. - Eur. J.* **2009**, *15*, 136−148. (d) Hisamatsu, Y.; Aoki, S. *Eur. J. Inorg. Chem.* **2011**, *2011*, 5360−5369. (e) Fan, C.; Li, Y.; Yang, C.; Wu, H.; Qin, J.; Cao, Y. *Chem. Mater.* **2012**, *24*, 4581−4587. (f) Xu, X.; Yang, X.; Dang, J.; Zhou, G.; Wu, Y.; Li, H.; Wong, W.-Y. *Chem. Commun.* **2014**, *50*, 2473−2476. (g) Zhao, J.; Yu, Y.; Yang, X.; Yan, X.; Zhang, H.; Xu, X.; Zhou, G.; Wu, Z.; Ren, Y.; Wong, W.-Y. *ACS Appl. Mater. Interfaces* **2015**, *7*, 24703−24714.
(36) (a) Tordera, D.; Bunzli, A. M.; Pertegas, A.; Junquera-Hernandez, J. M.; Constable, E. C.; Zampese, J. A.; Housecroft, C. E.; Orti, E.; Bolink, H. *Chem. - Eur. J.* **2013**, *19*, 8597−8609. (b) Constable, E. C.; Ertl, C. D.; Housecroft, C. E.; Zampese, J. A. *Dalton Trans.* **2014**, *43*, 5343−5356. (c) Ertl, C. D.; Gil-Escrig, L.; Cerdá, J.; Pertegás, A.; Bolink, H. J.; Junquera-Hernández, J. M.; Prescimone, A.; Neuburger, M.; Constable, E. C.; Ortí, E.; Housecroft, C. E. *Dalton Trans.* **2016**, *45*, 11668.
(37) You, Y.; Park, S. Y. *J. Am. Chem. Soc.* **2005**, *127*, 12438−12439.
(38) Suzuki, H.; Abe, H. *Tetrahedron Lett.* **1995**, *36*, 6239−6242.
(39) Zhu, W.; Ma, D. *J. Org. Chem.* **2005**, *70*, 2696−2700.
(40) Bian, M.; Xu, F.; Ma, C. *Synthesis* **2007**, *2007*, 2951−2956.
(41) Jitchati, R.; Batsanov, A. S.; Bryce, M. R. *Tetrahedron* **2009**, *65*, 855−861.
(42) Jacob, P.; Shulgin, A. T. *J. Med. Chem.* **1981**, *24*, 1348−1353.
(43) (a) Nonoyama, M. *Bull. Chem. Soc. Jpn.* **1974**, *47*, 767−768. (b) Lin, C.-H.; Chiu, Y.-C.; Chi, Y.; Tao, Y.-T.; Liao, L.-S.; Tseng, M.-R.; Lee, G.-H. *Organometallics* **2012**, *31*, 4349−4355.
(44) You, Y.; Seo, J.; Kim, S. H.; Kim, K. S.; Ahn, T. K.; Kim, D.; Park, S. Y. *Inorg. Chem.* **2008**, *47*, 1476−1487.
(45) (a) Chao, K.; Shao, K.; Peng, T.; Zhu, D.; Wang, Y.; Liu, Y.; Su, Z.; Bryce, M. R. *J. Mater. Chem. C* **2013**, *1*, 6800−6806. (b) Marchi, E.; Sinisi, R.; Bergamini, G.; Tragni, M.; Monari, M.; Bandini, M.; Ceroni, P. *Chem. - Eur. J.* **2012**, *18*, 8765−8773. (c) Li, T.-Y.; Jing, Y.-M.; Liu, X.; Zhao, Y.; Shi, L.; Tang, Z.; Zheng, Y.-X.; Zuo, J.-L. *Sci. Rep.* **2015**, *5*, 14912.
(46) Hay, P. J. *J. Phys. Chem. A* **2002**, *106*, 1634−1641.
(47) Tsuboyama, A.; Iwawaki, H.; Furugori, M.; Mukaide, T.; Kamatani, J.; Igawa, S.; Moriyama, T.; Miura, S.; Takiguchi, T.; Okada, S.; Hoshino, M.; Ueno, K. *J. Am. Chem. Soc.* **2003**, *125*, 12971−12979.
(48) Connelly, N. G.; Geiger, W. E. *Chem. Rev.* **1996**, *96*, 877−910.
(49) Jou, J.-H.; Wang, W.-B.; Shen, S.-M.; Kumar, S.; Lai, I.-M.; Shyue, J.-J.; Lengvinaite, S.; Zostautiene, R.; Grazulevicius, J. V.; Grigalevicius, S.; Chen, S.-Z.; Wu, C.-C. *J. Mater. Chem.* **2011**, *21*, 9546−9552.
(50) (a) Takizawa, S.; Shimada, K.; Sato, Y.; Murata, S. *Inorg. Chem.* **2014**, *53*, 2983−2995. (b) Sun, Q.; Mosquera-Vazquez, S.; Lawson Daku, L. M.; Guenee, L.; Goodwin, H. A.; Vauthey, E.; Hauser, A. *J. Am. Chem. Soc.* **2013**, *135*, 13660−13663.
(51) Murawski, C.; Leo, K.; Gather, M. C. *Adv. Mater.* **2013**, *25*, 6801−6827.
(52) Sharma, R. K.; Katiyar, M.; Kameshwar Rao, I. V.; Narayanan Unni, K.; Deepak, K. N. *Phys. Chem. Chem. Phys.* **2016**, *18*, 2747−2755.
(53) Frisch, M. J.; Trucks, G. W.; Schlegel, H. B.; Scuseria, G. E.; Robb, M. A.; Cheeseman, J. R.; Scalmani, G.; Barone, V.; Mennucci, B.; Petersson, G. A.; Nakatsuji, H.; Caricato, M.; Li, X.; Hratchian, H. P.; Izmaylov, A. F.; Bloino, J.; Zheng, G.; Sonnenberg, J. L.; Hada, M.; Ehara, M.; Toyota, K.; Fukuda, R.; Hasegawa, J.; Ishida, M.; Nakajima, T.; Honda, Y.; Kitao, O.; Nakai, H.; Vreven, T.; Montgomery, J. A., Jr.; Peralta, J. E.; Ogliaro, F.; Bearpark, M.; Heyd, J. J.; Brothers, E.; Kudin, K. N.; Staroverov, V. N.; Kobayashi, R.; Normand, J.; Raghavachari, K.; Rendell, A.; Burant, J. C.; Iyengar, S. S.; Tomasi, J.; Cossi, M.; Rega, N.; Millam, J. M.; Klene, M.; Knox, J. E.; Cross, J. B.; Bakken, V.; Adamo, C.; Jaramillo, J.; Gomperts, R.; Stratmann, R. E.; Yazyev, O.; Austin, A. J.; Cammi, R.; Pomelli, C.; Ochterski, J. W.; Martin, R. L.; Morokuma, K.; Zakrzewski, V. G.; Voth, G. A.; Salvador, P.; Dannenberg, J. J.; Dapprich, S.; Daniels, A. D.; Farkas, O.; Foresman, J. B.; Ortiz, J. V.; Cioslowski, J.; Fox, D. J. *Gaussian 09*, Revision A.02; Gaussian, Inc: Wallingford, CT, 2009.
(54) (a) Becke, A. D. *J. Chem. Phys.* **1993**, *98*, 5648−5652. (b) Lee, C.; Yang, W.; Parr, R. G. *Phys. Rev. B: Condens. Matter Mater. Phys.* **1988**, *37*, 785−789.
(55) (a) Dunning, T. H., Jr.; Hay, P. J. *Modern Theoretical Chemistry*; Schaefer, H. F., III, Ed.; Plenum: New York, 1976; Vol. 3. (b) Hay, P. J.; Wadt, W. R. *J. Chem. Phys.* **1985**, *82*, 270−283. (c) Wadt, W. R.; Hay, P. J. *J. Chem. Phys.* **1985**, *82*, 284−298. (d) Hay, P. J.; Wadt, W. R. *J. Chem. Phys.* **1985**, *82*, 299−310.
(56) (a) Petersson, G. A.; Al-Laham, M. A. *J. Chem. Phys.* **1991**, *94*, 6081−6090. (b) Petersson, G. A.; Bennett, A.; Tensfeldt, T. G.; Al-Laham, M. A.; Shirley, W. A.; Mantzaris, J. *J. Chem. Phys.* **1988**, *89*, 2193−2218.
(57) M'hamedi, A.; Batsanov, A. S.; Fox, M. A.; Bryce, M. R.; Abdullah, K.; Al-Attar, H. A.; Monkman, A. P. *J. Mater. Chem.* **2012**, *22*, 13529−13540.
(58) Tavasli, M.; Moore, T. N.; Zheng, Y.; Bryce, M. R.; Fox, M. A.; Griffiths, G. C.; Jankus, V.; Al-Attar, H. A.; Monkman, A. P. *J. Mater. Chem.* **2012**, *22*, 6419−6428.
(59) Allouche, A. R. *J. Comput. Chem.* **2011**, *32*, 174−182.
(60) O'Boyle, N. M.; Tenderholt, A. L.; Langner, K. M. *J. Comput. Chem.* **2008**, *29*, 839−845.

DOI: 10.1021/acs.inorgchem.6b01179
Inorg. Chem. 2016, 55, 8612−8627